metals

Review

Review on Laser Shock Peening Effect on Fatigue of Powder Bed Fusion Materials

Francisco Bumba [1], Paulo Morais [2], Rodolfo Batalha [2], Vitor Anes [1,3,4,*] and Luis Reis [1]

[1] IDMEC, Instituto Superior Técnico, Universidade de Lisboa, 1049-001 Lisboa, Portugal; francisco.paca@tecnico.ulisboa.pt (F.B.); luis.g.reis@tecnico.ulisboa.pt (L.R.)
[2] ISQ, Taguspark-Oeiras, 2740-120 Porto Salvo, Portugal; pjmorais@isq.pt (P.M.); rlbatalha@isq.pt (R.B.)
[3] Instituto Superior de Engenharia de Lisboa, 1959-007 Lisboa, Portugal
[4] Instituto Politécnico de Lisboa, 1549-020 Lisboa, Portugal
* Correspondence: vitor.anes@isel.pt

Abstract: The ability to manufacture parts with complex geometry by sending a model from CAD directly to the manufacturing machine has attracted much attention in the industry, driving the development of additive manufacturing technology. However, studies have shown that components manufactured using additive manufacturing technology have several problems, namely high tensile residual stresses, cracks, and voids, which are known to have a major impact on material performance (in service). Therefore, various post-treatment methods have been developed to address these drawbacks. Among the post-treatment techniques, laser shock peening (LSP) is currently considered one of the most efficient post-treatment technologies for improving the mechanical properties of materials. In practice, LSP is responsible for eliminating unfavorable tensile residual stresses and generating compressive residual stresses (CRS), which result in higher resistance to crack initiation and propagation, thus increasing component life. However, since CRS depends on many parameters, the optimization of LSP parameters remains a challenge. In this paper, a general overview of AM and LSP technology is first provided. It then describes which parameters have a greater influence during powder bed melting and LSP processing and how they affect the microstructure and mechanical properties of the material. Experimental, numerical, and analytical optimization approaches are also presented, and their results are discussed. Finally, a performance evaluation of the LSP technique in powder bed melting of metallic materials is presented. It is expected that the analysis presented in this review will stimulate further studies on the optimization of parameters via experimental, numerical, and perhaps analytical approaches that have not been well studied so far.

Keywords: laser shock peening; powder bed fusion; fatigue; residual stress

check for updates

Citation: Bumba, F.; Morais, P.; Batalha, R.; Anes, V.; Reis, L. Review on Laser Shock Peening Effect on Fatigue of Powder Bed Fusion Materials. *Metals* **2023**, *13*, 1762. https://doi.org/10.3390/met13101762

Academic Editor: Vadim Sufiiarov

Received: 20 September 2023
Revised: 10 October 2023
Accepted: 12 October 2023
Published: 17 October 2023

1. Introduction

According to the International Organization for Standardization/American Society for Testing and Materials in ISO/ASTM 52900:21, additive manufacturing is defined as "a process for joining materials to create physical objects specified by 3D model data" [1]. Unlike conventional manufacturing methods, which are subtractive, additive manufacturing sends data from CAD to the machine, and the part is made layer by layer until it is finished.

Recently, additive manufacturing technology is gaining momentum in various industries, such as aerospace [2,3], automotive [4], biomedical [5,6], and marine [7]. According to a report by Grand View Research, the global market for metal 3D printing is estimated at USD 656.5 million, with nearly 50% of this technology in the aerospace and defense industry, as shown in Figure 1, which was plotted using data collected from the report [8]. In another report by the same institute, the market for AM technology is expected to reach USD 76.16 billion by 2030 [9].

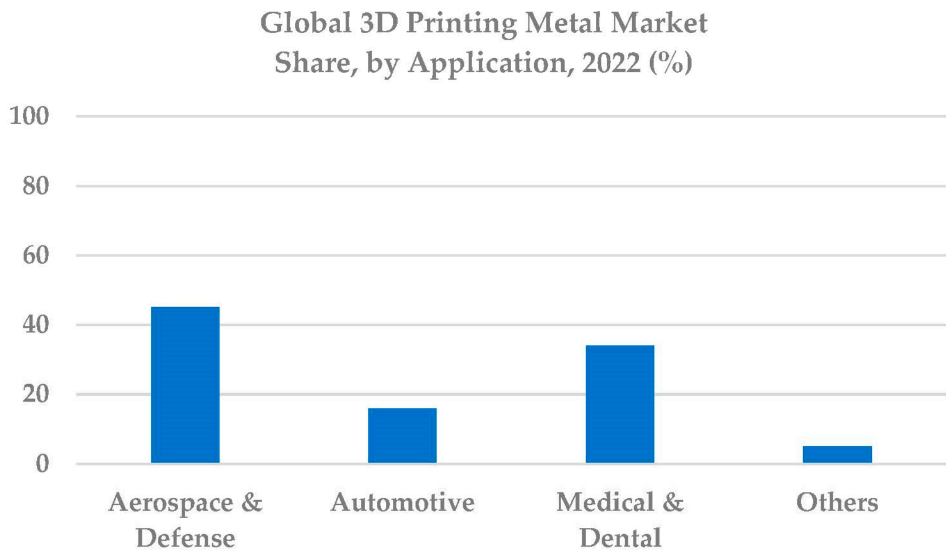

Figure 1. Market share of additive manufacturing in several industries.

There are many reasons for the increasing use of AM technology, for example, its ability to produce components with complex geometry in a single step, which is very difficult and sometimes impossible with conventional manufacturing technologies. Another major advantage of AM is that components are built layer by layer, which allows for more efficient use of materials because no material is wasted. In addition, AM methods can produce lighter components, which is highly valued in the aerospace industry, where a combination of safety and weight is important. Many other reasons contribute to the exploration of AM technology. The fact that a model is sent directly from CAD to the AM machine to produce a part helps save a lot of time by eliminating intermediate steps normally involved in conventional manufacturing, thus reducing time to market.

Many AM techniques have been developed, but they are all based on the same basic principle: a component is built up layer by layer until the component is complete. According to ASTM [1], additive manufacturing processes are divided into the following categories: material jetting, VAT polymerization, binder jetting, powder bed fusion, sheet lamination, and directed energy deposition, as shown in Figure 2.

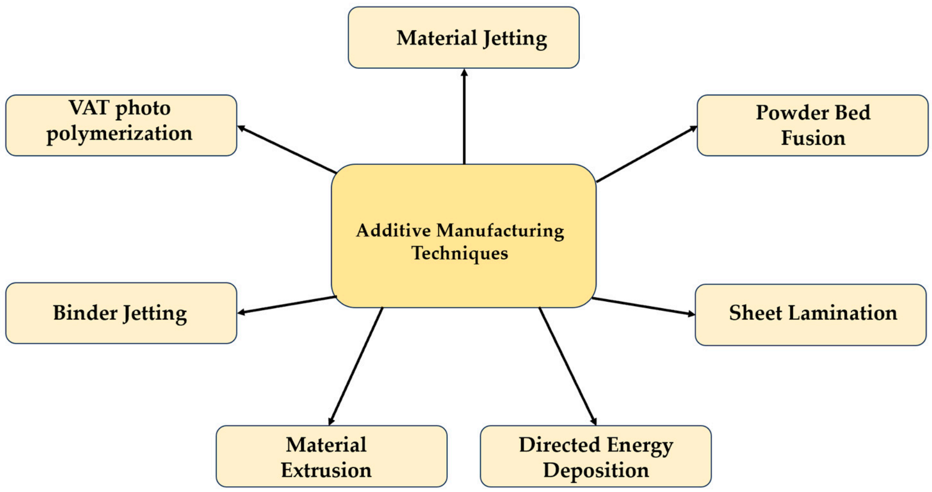

Figure 2. Additive manufacturing techniques.

In the early stages of AM technology development, the focus was on paper laminates, waxes, and polymers, but in subsequent years, the scope expanded to include other types of materials such as metals, composites, and ceramics. The AM techniques shown in

Figure 2 can process all of these materials, but there are specific techniques that are best suited for each type of material. For example, for metallic materials, PBF, sheet lamination, binder jetting, and directed energy deposition are best suited, which is referred to as metallic additive manufacturing (MAM). In practical engineering applications, ensuring the reliability and safe operation of additively manufactured components is important, particularly for components that include notch features since the areas of geometrical discontinuities are recognized as stress concentration points. To ensure the integrity of AM-built components, Niu et al. [10] proposed a defect-tolerant approach that considers size effect, notch effect, and fatigue scatter. One great advantage of the proposed approach is the ability to estimate the AM part allowable defect size, and it has been shown that the size effect influences the lifetime of components [11].

Although the use of AM technology offers great advantages over conventional manufacturing processes, parts produced with AM processes still have shortcomings, such as surface defects, void formation, undesirable residual stresses, and anisotropic microstructure. All of these problems are known to negatively impact part strength and shorten part life. To counteract the problems associated with AM, several researchers have conducted several studies. For example, Gong et al. [12] studied the SLM samples of Ti6Al4V intentionally fabricated with defects by changing the manufacturer's standard parameters to find an explanation for the defect formation. Based on the porosity results, a process window was created with four zones: "completely dense" (zone I), "overmelting" (zone II), "incomplete melting" (zone III), and "overheating" (zone OH) to show how the process parameters affect defect formation. Among these zones, it has been shown that only Zone I samples, which are free of porosity, can be produced with specific parameters that must be tuned to the material [13]. According to Li et al. [14], there are more than 100 parameters in the literature that affect the performance of an additively manufactured material. For this reason, it is not possible to solve the AM problems only by an optimization process.

To extend the lifetime of components manufactured with AM techniques, numerous surface post-treatment techniques have been developed, namely heat treatment (HT), hot isostatic pressing (HIP), nanocrystalline surface modification with ultrasound (UNSM), shot peening (SP), and LSP. Among the post-treatment methods, heat treatment is used to reduce the residual stresses generated in AM processes due to the high thermal gradient and rapid cooling rate. HIP has been successfully used to reduce porosity in IN718 [15,16], and the reduction in porosity resulted in an increase in lifetime. While the authors [17] found in one study that treatment with HIP alone improved fatigue strength by more than 100% compared to printed and stress-relieved specimens, in another study, better fatigue performance was achieved by stress relief rather than a combination of SR and HIP [18]. The authors concluded that the reduction in fatigue life was due to the presence of surface defects during HIP and that the complete elimination of pores was not achieved even at pressures greater than 100 MPa. Studies conducted with other post-processing methods such as UNSM [19], SP [20,21], and LSP [22] have shown that they were able to improve fatigue life by introducing CRS as well as by creating grain refinement.

Among all these surface post-treatment methods, LSP is currently considered one of the most efficient post-treatment technologies for improving the mechanical properties of the materials. Several advantages are associated with LSP technology. For example, Plessis et al. [23] applied the LSP technique to AlSi10Mg prepared by laser powder bed fusion (LPBF). The results showed that the LSP technique is able to close surface pores. It is known that areas with pores usually act as crack initiators, so LSP increases the fatigue strength of the material. Compared to SP, LSP treatment results in CRS with higher stability because it causes less cold deformation. Moreover, the LSP method achieves greater CRS depth [24]. In addition, LSP treatment allows the application of shock peening to components with different geometries as well as in certain areas of complex geometries that cannot be achieved with other surface treatments, which increases component lifetime. Since the CRS produced by LSP depends on the LSP parameters, they can be modified to produce a desired compressive residual stress field and avoid tensile stresses at critical locations.

There are many general reviews of the application of LSP surface treatment [25–28] to materials produced by conventional methods. A review of the effects of LSP on AM metals was written by Munther et al. [29], and in another review, the authors focused on LSP on materials prepared by PBF and laser-based directed energy deposition [30]. Recently, many other studies have been conducted on the application of LSP to PBF materials. In this review, these studies are added and discussed. Moreover, it is well known that the LSP optimization process is still a problem to be solved and there are not many reviews focusing on the optimization process. In this review, a brief introduction to AM and LSP is first given, followed by a description of some aspects of the PBF method, including the microstructure, mechanical properties, and residual stress of PBF materials. The effects of LSP on microstructure, mechanical properties, and residual stress are also examined. Experimental, numerical, and analytical optimization approaches are also presented, and their results are discussed. Finally, a performance evaluation of LSP technique in powder bed melting of metallic materials is presented.

2. Powder Bed Fusion Process

2.1. PBF Working Principle

Powder Bed Fusion is known as the first commercially available AM technology; it is also the most widely used AM process for metallic materials. The operating principle of PBF is shown in Figure 3. The process takes place in a 3D printer with a controlled atmosphere (under argon/nitrogen), so that oxidation can be avoided during the process and the powder can be deposited after each layer. The PBF device also consists of a build plate, also called a substrate, which is usually made of metal. The powdered material is applied to the build plate in a thin layer using a roller. Then, energy from a heat source is directed specifically to melt the powder on the substrate and create a cross-section of that layer. The process continues layer by layer until the complete component is finished.

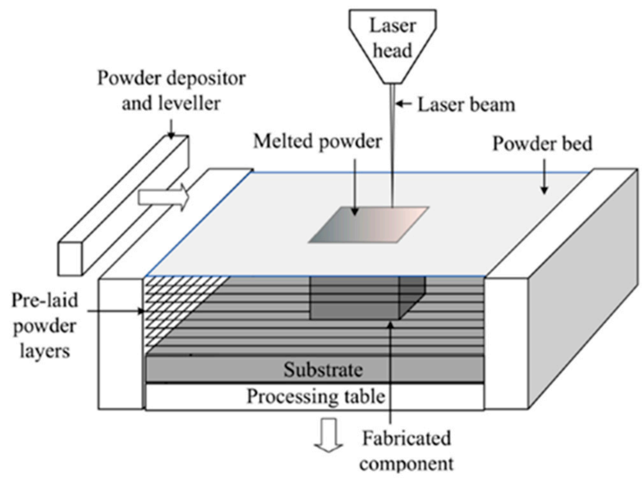

Figure 3. PBF schematic [31].

PBF technology usually uses an electron beam gun or a laser beam as an energy source, but other types of thermal energy sources can also be used. The most commonly used energy source in PBF is lasers. Many types of PBF technology have been developed, the most common of which are Selective Laser Sintering (PBF-LB/P, SLS), Electron Beam Melting (PBF-EB/M, EBM), Selective Laser Melting (PBF-LB, SLM), Selective Heat Sintering (SHS), Multi Jet Fusion (PBF-IrL/P, MJF), and Direct Metal Laser Sintering (DMLS). The full description of each of these PBF variants can be found in [32].

As for the materials to be used for PBF, materials that can be melted and re-solidified are suitable for this method. The most commonly used metals in PBF are steel, stainless steel, nickel-based alloys, aluminum, and titanium. Despite their great advantages, PBF components, like all AM techniques, also have some internal and external defects, namely high tensile residual stresses [33,34] anisotropic and inhomogeneous microstructure [35], a high degree of surface roughness [34], and porosity [12,36,37]. The fatigue performance of as-built materials is greatly affected by the combined effects of the as-built defects in the materials.

2.2. Processing Parameters

The success of PBF processing depends on many parameters, as shown in Figure 4. For this reason, PBF parameters are usually optimized to ensure a high quality of the final product. Often, PBF machine manufacturers offer their customers optimized parameters for a specific condition.

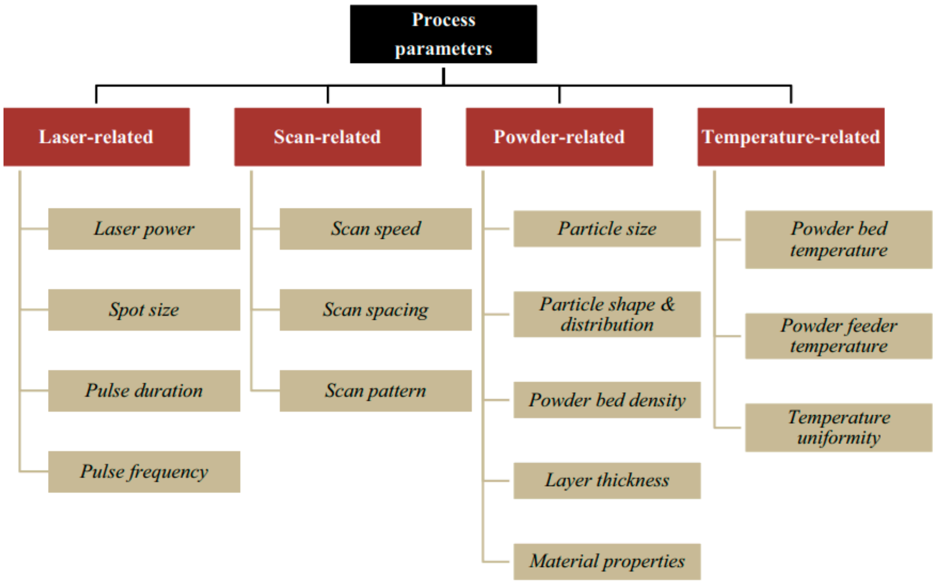

Figure 4. PBF processing parameters [36].

The dependence of the final product on many parameters increases the complexity of the process. For this reason, Jia et al. [38,39] and Sateesh et al. [40] combine laser power, scan speed, hatch spacing, and layer thickness/beam diameter into a single parameter called volumetric energy density, laser energy density, and linear laser energy density. For example, in the SLM process, the scan speed, laser power, hatch spacing, and layer thickness have the most influence [36], and many studies have used these parameters to increase the density of the final product [41,42]. The processing parameters in the PBF process can be calculated using the following equations:

$$E = \frac{P}{v\delta} \quad (1)$$

$$\eta = \frac{P}{v} \quad (2)$$

$$\varepsilon = \frac{P}{vhd} \quad (3)$$

where E is the energy density in J/mm^2, P is the laser power in J/s; v is the scan speed in m/s; δ is the hatch spacing in mm, η is the linear energy density in J/mm, ε is the volumetric energy density in J/mm^3; h is the hatch spacing in µm; and d is the layer thickness in µm.

2.3. Mechanical Properties

To understand how build orientations and HT affect both the microstructure and mechanical properties of additively manufactured IN718, dog bone specimens were fabricated with four different build orientations 0°, 45°, 55°, and 90° [43]. The results of tensile tests showed that the highest yield stress and UTS were obtained at 55°, followed by 90°, while the highest elongation was observed at 45°. The results also showed that higher mechanical properties were obtained for vertically fabricated specimens than for horizontal specimens, which is contrary to the results obtained by Podgornk et al. [44] and Alsalla et al. [45].

Regarding aluminum alloys, Read et al. [46] studied the influence of the parameters used in the SLM process. The mechanical properties of the study were obtained using optimized parameters determined using a statistical approach called the design of experiments. Two different buildup directions (horizontal and vertical) were considered in this study. From the results of the tensile properties (see Figure 5), it was concluded that the buildup direction has only a minor influence on the tensile properties. However, compared to the die-casting alloy A360, higher tensile strength properties were obtained for both the vertical and horizontal orientations BD, except for elongation, which is three times lower. Table 1 shows the tensile strength properties of the specimens produced with different BD.

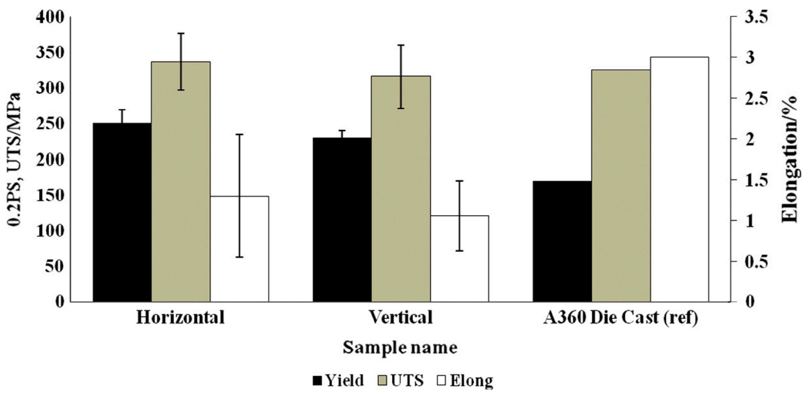

Figure 5. Comparison of tensile properties of SLM fabricated samples and die-cast A360 alloy [46].

Table 1. Tensile properties of PBF materials.

Materials	UTS (MPa)			YS (MPa)			E (%)		
	0°	45°	90°	0°	45°	90°	0°	45°	90°
316L [45]	668		564	397		387	37		35
MS1 [44]	2000	2020	1850	1940	1935	1915	5	4.6	4.8
316L [47]	630–635		610–630	460–475		450–470	50		60
Ti6Al4V [48]	833		851	783		812	2.7		3.6

3. Laser Shock Peening

3.1. Fundamentals of LSP

Laser shock peening (LSP) is a surface treatment method for improving the mechanical properties of materials. The LSP method improves material properties by eliminating harmful tensile stresses and introducing plastic deformation and positive CRS, resulting in higher resistance to crack propagation and initiation, thus increasing the life of a component.

The operating principle of the LSP technique is shown in Figure 6 and the respective formulations are presented in Equations (4)–(7) [27]. The process begins with the application of a constraint layer and a sacrificial layer to the material being processed. As shown in Figure 6, the laser beam penetrates the barrier layer, which is transparent to the laser beam, and strikes the surface of the workpiece, creating a plasma. The transparent layer traps the plasma and transfers the energy generated by the plasma to the material, creating a shock wave that results in residual stresses in the material. The sacrificial layer applied to the material is responsible for absorbing the laser energy and protecting the workpiece from damage.

$$\frac{dL(t)}{dt} = \frac{2P(t)}{Z} \tag{4}$$

where Z is the reduced shock impedance, which can be determined by

$$\frac{2}{z} = \frac{1}{Z_s} + \frac{1}{Z_t} \tag{5}$$

where Z_t is the shock impedance of the target material, Z_s is the shock impedance of the confined material, and I is the laser intensity. The laser intensity satisfies Equation (6).

$$I(t) = \frac{P(t)dL}{dt} + \frac{3d[P(t)L(t)]}{2\alpha dt} \tag{6}$$

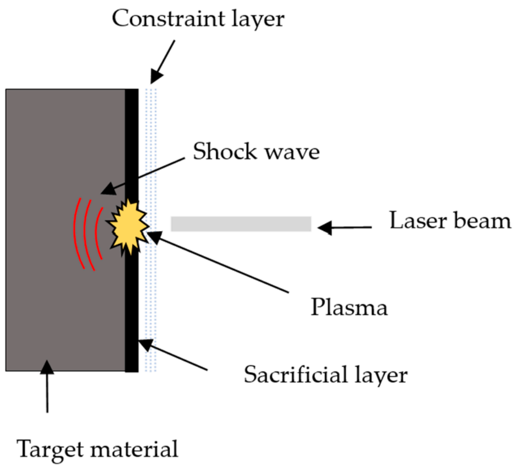

Figure 6. LSP Process.

The peak pressure can be calculated using the following equation:

$$P = 0.1\sqrt{\frac{\alpha}{2\alpha + 3}}\sqrt{Z}\sqrt{I} \tag{7}$$

Studies by Takata [49] and Xiong [50] have shown that the choice of material for the sacrificial and boundary layers affects the pressure generated by the shock wave. Various materials such as glass [51], quartz [49,51–54], and water [55–57] are usually used for the boundary layer. However, among these materials, water is the preferred choice because it is cheap and can be easily integrated into the overall structure of the LSP. On the other hand, aluminum [58,59], copper [60], zinc [61], lead [53], vinyl tape [62–64], black tape [65,66], and black paint [67,68] have been used for the sacrificial layer. A study conducted in 1998 showed that black paint provides the best absorption for standard LSP (wavelengths 1064 nm and 532 nm) [69].

The ability of LSP to extend component life has been demonstrated in many industrial applications. For example, general electric used LSP to treat a gas turbine rotor operating at high speeds, which resulted in high tensile and vibratory stresses in the blade and made it susceptible to foreign object damage events (FOD) [70]. The application of LSP resulted in extended fan blade life and increased resistance to foreign body damage (FOD). Toshiba used underwater LSP without coating (LSPwC) to solve stress corrosion cracking problems in nuclear reactors [71].

3.2. Laser Parameters and Residual Stress

Withers et al. [72] classified residual stresses with respect to different length scales. The classification includes type I (macro stresses), type II (grain scale), and type III (atomic scale). The origin of Type I residual stresses is the non-uniform plastic deformation introduced into the material during the manufacturing process, whereas Type II and III residual stresses are due to the presence of defects, namely impurities, dislocations, and porosity, in the material. For PBF materials, it has been discussed that the presence of tensile residual stresses is one of the main causes of poor fatigue performance of the components. There are numerous techniques for measuring residual stresses, including drilling, electron diffraction, X-ray diffraction, ultrasonic methods, magnetic methods, and nanoindentation methods. The non-destructive X-ray method is the method preferred by the scientific community. There are other methods for residual stress measurement, the detailed description and comparison of which can be found in [73,74]. For PBF materials treated with LSP, X-ray diffraction is the most used method, followed by the hole-drilling method.

3.3. Laser Power Density

There is a direct proportionality relationship between the pressure of the shock wave and the power density of the laser, i.e., an increase in the power density of the laser leads to an increase in the shock wave and thus to an increase in CRS, a schematic of CRS is shown in Figure 7. To create residual stresses in the material, the value of the laser power density should be 2–2.5 greater than HEL.

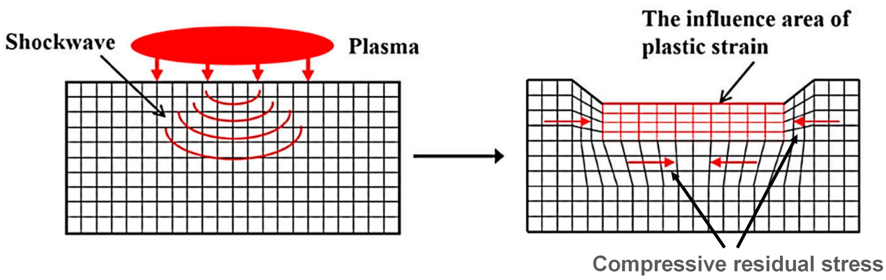

Figure 7. Schematic of compressive residual stress [75].

In a study on additively manufactured AlSi10Mg, two different laser power densities (3 and 9 GWcm^{-2}) were used for LSP treatment [76]. The sample used in this study was both heat-treated and LSP-treated. The residual stress distribution results obtained in this study are shown in Figure 8. From the result, it can be seen that the highest CRS value was obtained for the untreated samples treated with higher laser power density (AB + LSP2). Even considering the HT effect, it can be seen that the largest CRS value was obtained for the hybrid treatment with higher laser power density (AB + HT + LSP2).

The most appropriate value for laser power density for a particular application can be determined using an optimization process. It is important to note that there is a saturation point beyond which further increases in laser power density will stabilize or even decrease CRS rather than increase it.

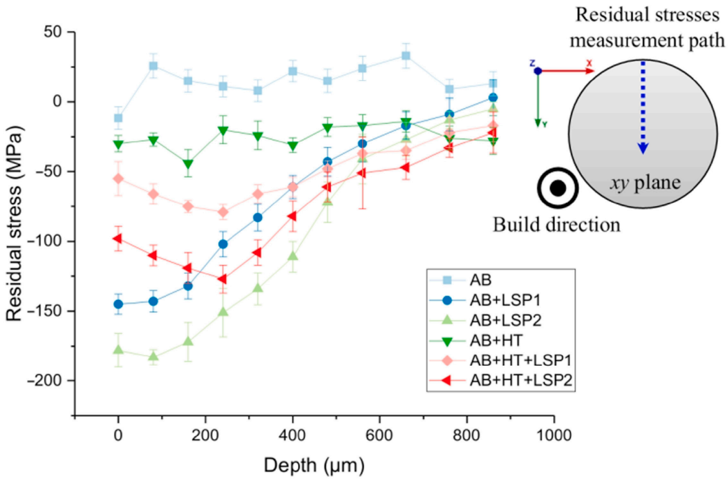

Figure 8. Residual stress distribution in y-component (perpendicular to the building direction) [76].

3.4. Spot Size and Shape

The spot size is an important parameter that directly affects the depth and size of CRS. Monstross et al. [77] pointed out that two different behaviors of the shock wave can occur depending on the size of the spot. For a large spot diameter, the shock wave behaves like a plane front with an attenuation rate of 1/r, whereas for a small spot diameter, a spherical shock wave expansion is achieved with an attenuation rate of 1/r2. Therefore, the lower attenuation behavior at a large spot diameter leads to further propagation in the material.

The diameter of the laser spot is related to the laser intensity by Equation (8). From this equation, it can be seen that an increase in the spot diameter leads to a decrease in the laser intensity. However, the value of laser intensity can be recovered even if the laser energy is increased. The inverse relationship between the laser intensity and the diameter of the laser spot states that a smaller spot size should result in a higher CRS.

$$I_o = \frac{4E}{\pi D^2 \tau} \tag{8}$$

where E is the pulse energy in J, τ is the pulse width in ns, and D is the laser spot diameter in cm. When applying LSP in PBF material, the round spot shape is most commonly used, followed by square shapes. However, by varying the angle of incidence of the LSP device, other shapes such as rectangular and elliptical can be obtained. To investigate how the spot size affects the residual stress in SLM components, Kalentics et al. [78] conducted a study considering three different spot sizes with diameters of 1 mm, 2 mm, and 5 mm. The results of this study showed that, on the one hand, the magnitude of the residual compressive stress decreases with increasing spot size, and, on the other hand, the increase in spot size leads to an increase in the depth of CRS.

3.5. Overlapping Rate

Throughout the LSP treatment, the overlap rate plays a very important role in ensuring that CRS is evenly distributed throughout the material. The proper distribution of CRS also helps prevent unwanted damage and excessive heating in certain areas of the material. The overlap rate can be calculated using Equation (9).

$$\eta = \frac{Cl}{D} \times 100\% \tag{9}$$

where Cl and D denote the coincidence length of the consecutive spots and laser spot diameter. During the LSP process, the overlap rate is controlled by moving the target material fixed on the table in the x-y direction. Karbalaian et al. used FEM to investigate the effects of overlap on LSP [79]. A square shape of the laser spot and an overlap of 0–80%

were considered. The results of this study showed that the computational cost increases with the overlap rate. This result means that the financial aspect should also be considered when selecting the overlap rate.

In another study, Luo et al. [80] conducted a 3D finite element modeling study for Al alloy LY2 and considered four different overlap percentages of 30%, 50%, 70%, and 90% (see Figure 9) to better understand their influence on residual stress and surface deformation under massive LSP actions. From the results, it was concluded that the depth of residual stress increases with the degree of overlap.

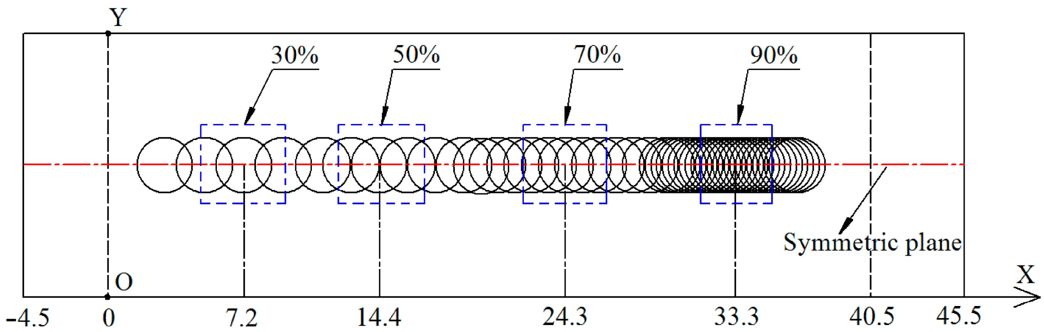

Figure 9. Four different overlapping percentages [80].

3.6. Wavelength

Normally, three wavelengths are considered in LSP: 1064 nm (near-infrared), 532 nm (green), and 355 nm (ultraviolet). Of these wavelengths, 1064 nm is most commonly used for LSP applications on materials fabricated with both traditional and AM technologies (see Table 2). The near-infrared wavelength of 1064 nm is the most used due to the high absorption of water.

Some LSP applications are performed underwater. In this case, the second harmonic of 532 nm is usually used, and no protective layer is applied [25]. However, Yeo et al. applied LSP post-treatment with the second harmonic 532 nm to improve the surface properties of heat-treated Ti6A14V fabricated with LPBF [81]. The residual stress results showed that the LSP application significantly improved the material properties by producing a CRS that is 6 times higher than that of the sample HT, about 2.6 times higher than that of the sample that received surface milling treatment, and more than 10 times higher than that of the as-built sample. Table 2 provides a summary of some LSP processing parameters used in PBF-manufactured materials, including some very recent studies.

Table 2. LSP parameters applied in PBF materials.

Material	F [Hz]	D_p [mm]	λ [nm]	E [J]	D_{spot} [mm]	O (%)	Constraint Layer (Thickness)	Sacrificial Layer (Thickness)
Ti-6A1-4V [58]	10	10		7.6	2	50	Water (1 mm)	Al foil (500 µm)
PdPtRhIrCuNi [82]	5	6.3	1064	1.5	1.2	40, 80	Water	No sacrificial layer
Ti-6A1-4V [81]	10	8	532	1.4	1.34	50	Water	Al foil (100 µm)
AlSi7Mg [83]	5	6.3	1064	1	1	50	Water	
AlSi10Mg [76]	10	10	1064	1.5, 4.5		50	Water (2 mm)	
316L SS [84]	10	20	1064	3–5		30	Water	No sacrificial layer
316L SS [85]	5	6.3	1064	0.4	1	40	Water	
AlSi10Mg [86]	10	10	1064	4.5		50	Water (2 mm)	Al foil (200 µm)
Zr-based bulk mettalic glass [87]	5	6.3	1064	1.5	1.2	50	Water	No sacrificial layer
Ti-6A1-4V [88]		10	1064	9	3	50	Water (1 mm)	Al foil (100 µm)
Ti-6A1-4V [89]	5	10	1064	7.6	3	50	Water (1 mm)	Al foil (100 µm)
Ti-6A1-4V [56]		18			3 × 3	50	Water	Black tape
316L SS [90]		10	1064	9		50	Water	Al foil
IN625 [91]	5	10	1064	7	2.6	50	Water (1.5 mm)	Al foil (120 µm)
316L SS [92]		15	1064	3.5	2	75	Water (2 mm)	Black tape (110 µm)
CM247LC [93]	5	6.3	1064	0.4	1	80, 40, 80		Al tape (70 µm)
304L SS [64]	10	14		5	2 × 2		Water	Vinyl tape (130 µm)
Ti-6A1-4V [94]	10	6	1064	0.35	0.8		Water (submerged sample)	Glass chamber (3 mm)
Ti-6A1-4V [95]		12	1064			25		Vinyl tape (130 µm)
316L SS [63]		10		4	3 × 3		Water	Al tape (90 µm)
15-5 PH SS [66]	10	10	1064	0.8		80, 30	Water (2 mm)	PVC black tape (125 µm)
Ti-6A1-4V [96]		18			3	50	Water	Black tape

Note: F is the frequency, D_p is the pulse duration, λ is the wavelength, E is the pulse energy, D_{spot} is the spot diameter, and O is the overlapping rate.

3.7. LSP Effect on Microstructure Surface Modifications

During LSP processing, the materials fabricated by both traditional and additive technologies undergo microstructural changes that are commonly characterized via scanning electron microscope (SEM), transmission electron microscope (TEM), and X-ray diffractometer. Since the LSP process depends on several parameters, the microstructural evolution observed in the material depends on both the heat treatment and the LSP parameters.

Guo et al. [96] investigated the effects of LSP on the microstructure evolution, microhardness, residual stress, and mechanical properties of Ti6Al4V prepared by AM technology. The microstructural changes before and after the LSP process were analyzed by optical microscopy, SEM, and TEM. In Figure 10a, the presence of few pores and refined equiaxed α-grains can be seen as a bright phase, whereas in Figure 10b, a purple phase with a refined layer of about 400 µm can be seen. In Figure 10c,d, the structure of the grains before and after LSP can be seen. Finally, Figure 10e,f show the calculated average values of the grain size distribution. The average value of grain size for Figure 10c,d is 33.6 µm and 24.3 µm; this decrease in grain size is due to LSP treatment.

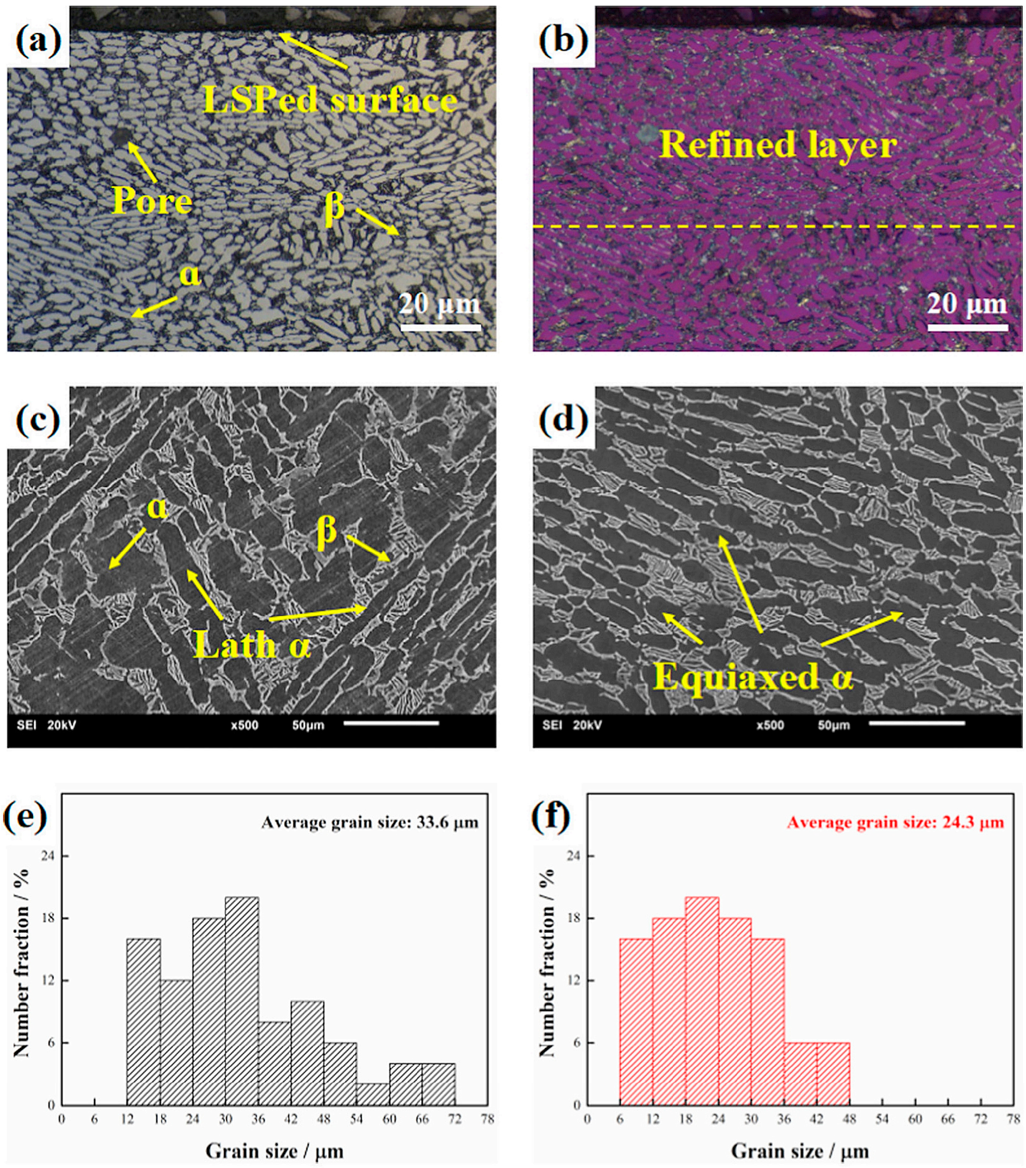

Figure 10. (**a**,**b**) Optical images of the cross-sectional area near the surface after LSP; (**c**,**d**) SEM image before and after LSP; (**e**,**f**) grain size distribution of α grain in (**c**,**d**) [96].

The authors also obtained TEM images of the samples before and after LSP, as shown in Figure 11. Before the application of LSP, as shown in Figure 11a, the sharp boundaries of the dark and light areas representing both primary α-phase and β-phase are clearly visible. The microstructural changes after LSP can be seen in Figure 11b–d. The boundaries of the α-phase and the β-phase are not very clearly visible. The mechanical twins (MTs) of 131 nm and 164 nm can be seen in Figure 11b,c. Dislocation lines (DLs) and dislocation tangles (DTs) can also be seen in Figure 11d. The presence of elements such as MTS, DLS, and DTs has also been observed in other LSP studies performed on components fabricated with PBF [56,91], and it is known that all these elements play an important role in the grain refinement process [97,98].

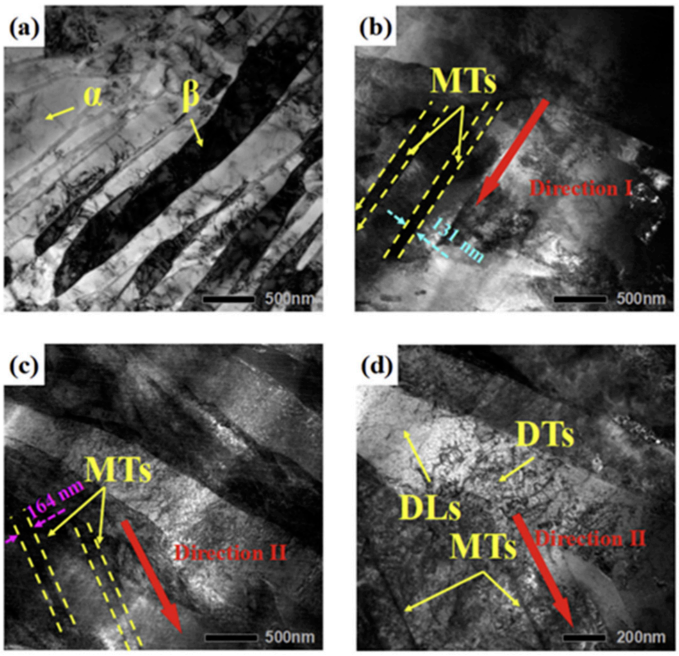

Figure 11. TEM images (**a**) before and (**b**–**d**) after LSP [96].

3.8. LSP Effect on Mechanical Properties of PBF Materials

Many researchers have reported that LSP applications can convert harmful residual stresses into beneficial compressive stresses, and LSP treatment also promotes grain refinement in materials. Both grain refinement generation and CRS are responsible for improving the mechanical properties of materials. LSP treatment in additively manufactured materials has shown different effects on the tensile properties of the materials. Table 3 summarizes some results of the tensile properties of PBF materials, and these results focus on comparing the mechanical properties of as-built (AB) samples, for the LSP-treated specimen as well as samples subjected to hybrid treatment (HT + LSP). The results of the mechanical properties presented in Table 3 were used to plot Figure 12, which shows the relationship between the samples before (AB) and after LSP treatment. From Figure 12a,b, it can be observed that the UTS and YS after LSP treatment (y-axis) is greater than those before LSP treatment (x-axis), and this improvement in mechanical properties is the result of both CRS and grain refinement produced by LSP. However, for the elongation, as illustrated by Figure 12c, a varying trend between tensile properties between AB and LSP samples is seen.

Table 3. Tensile property results of PBF materials.

Materials	UTS (MPa)			YS (MPa)			E (%)		
	AB	HT	LSP	AB	HT	LSP	AB	HT	LSP
IN625 [59]	836	927	1029	576	813	869	45.2	43.1	46
Ti64 [95]	1253.3		1286.7	1113.3		1156.7	7		6.5
Ti6Al4V [99]	953		1058	896		962	4.3		6.2
Tic/IN625 [91]	1204	1435	1517	641	769	784	42.9	40.6	44.5
Ti6Al4V [89]	1035		1183	865		952	9.55		11.3
AlSi10Mg [86]	375		418	270		321	3		2.82

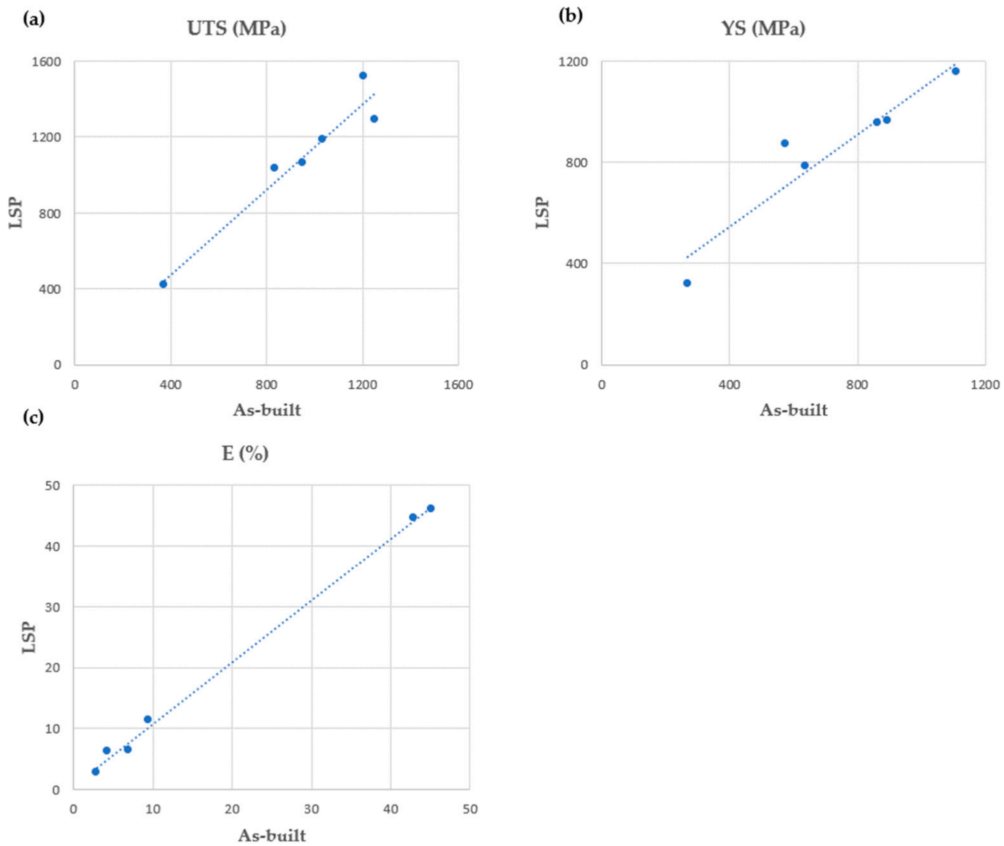

Figure 12. Tensile properties relationship between as-built and LSP samples: (**a**) UTS, (**b**) YS, and (**c**) E.

Deng et al. [90] conducted an experimental study on the effect of LSP on the tensile properties of 316L stainless steel produced by selective laser melting. The studied specimens were fabricated in three different directions of construction (0°, 45°, and 90°) and treated with LSP on both sides. The results of the tensile tests showed that both yield and tensile strength increased after LSP treatment, with the highest strength obtained for the 90° specimens. For elongation, a decrease was observed after LSP treatment at 0° and 45°, whereas LSP resulted in an increase in material elongation at 90°. The lowest value was found to be 5.7% for the horizontally treated specimens. In another study by Guo and co-workers [96], an increase in elongation of more than 50% was observed after LSP treatment for both horizontally and vertically prepared specimens. Contradictory results on tensile strength were also obtained in two studies investigating a hybrid treatment (HT, HT + LSP). In the first study, UTS increased with HT and continued to increase after the application of HT + LSP, whereas in the other study, UTS decreased when the specimens were subjected to different treatments (HT and HT + LSP).

3.9. LSP Parameter Optimization

One of the main objectives of using LSP technology is to generate a large amount of CRS, which increases the resistance of the material to the formation and propagation of cracks. Moreover, it has been shown that the depth of CRS depends on the LSP parameters, of which the laser power density/pulse energy seems to be the most influential parameter. Since the choice of LSP parameters affects the residual stresses generated, it is important to ensure that the laser-induced mechanical properties of the materials can actually be improved. To achieve this, researchers have optimized the LSP parameters. In this section, the optimization approach of some LSP studies is discussed.

Sun et al. used a model of a single-point laser shock created by the finite element method using ABAQUS [100]. The model was created to determine the optimal parameters for shock energy, laser pulse duration, and shock frequency for 20CrMnTi. The process of implementing the model is shown in the figure. As can be seen in Figure 13, the residual stress distribution and equivalent plastic deformation of the LSP-treated 20CrMnTi were simulated using explicit dynamic analysis along with explicit rebound analysis. As for the meshing of the cells, a refinement around the affected area with a diameter of 3 mm was performed.

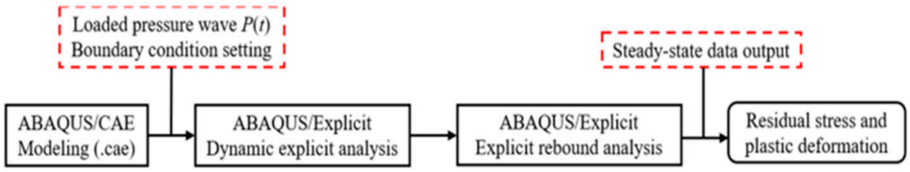

Figure 13. Step-by-step process of LSP simulation [100].

The optimal parameter is determined by varying the shock energy (4 J, 5 J, 6 J, and 7 J), laser pulse duration (10 ns, 15 ns, 20 ns, and 25 ns), and impact number (1–8 with an interval of 1). The optimal parameters obtained from the simulated results are 5 J, 20 ns, and 5 impact time. In another study, an artificial intelligence algorithm XGBoost was used to evaluate the mechanical properties and surface roughness of FGH4095 superalloy treated by LSP [101]. For this study, three different laser energies and two different overlapping rates were considered. The predicted results showed that higher surface roughness could be obtained by either increasing laser energy or considering lower overlapping rates. Finally, the findings concluded that a good agreement was obtained between the experimental and predicted results; however, a better LSP quality could be achieved by selecting higher laser energy and overlap rate and also considering the prepolishing of the shocked surface before LSP.

To determine the optimum value for LSP laser intensity, Ramadas et al. [66] used 15–5 precipitation-hardened stainless steel fabricated with LPBF and subjected to LSP treatment. The considered specimens were fabricated in two different directions (horizontal and vertical). The optimization process was performed by parametrically changing the laser power density (3.1 GW/cm^2, 4.5 GW/cm^2, and 7 GW/cm^2) and the number of LSP shots (1, 3, 5, and 7). Based on the residual stress results shown in Figure 14a,c, the optimal laser power density of 4.5 GW/cm^2 was determined since it provides the highest CRS value. For the number of shots, the optimal value was 5, as shown in Figure 14d. Using the optimized laser power density, samples with different thicknesses of 2 mm and 7 mm were subjected to LSP with multiple shots, and the results are shown in Figure 15. From Figure 15b, it can be seen that the depth of CRS is higher in the thicker samples than in the thinner ones. For both specimens, it can be observed that the depth of CRS increases with the number of shots.

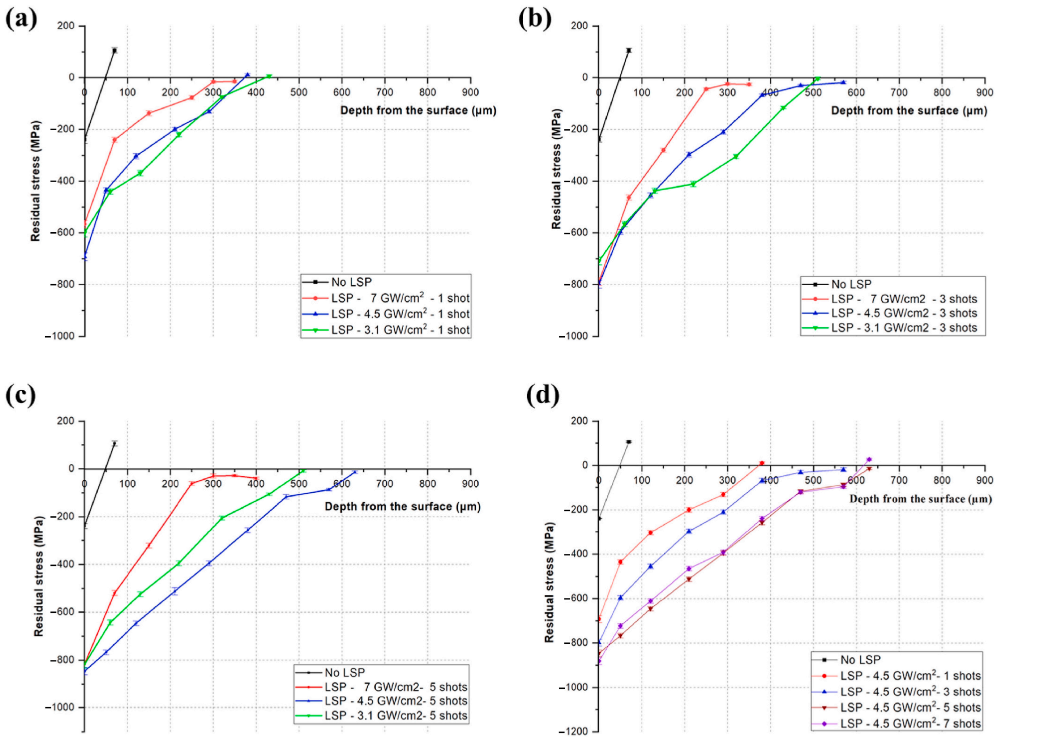

Figure 14. Residual stress distribution of LSP treated with (**a**) different laser intensity for 1 shot, (**b**) varying laser intensity with 3 shots, (**c**) varying laser intensity with 5 shots, and (**d**) laser intensity 4.5 GWcm^{-2} with varying laser intensity [66].

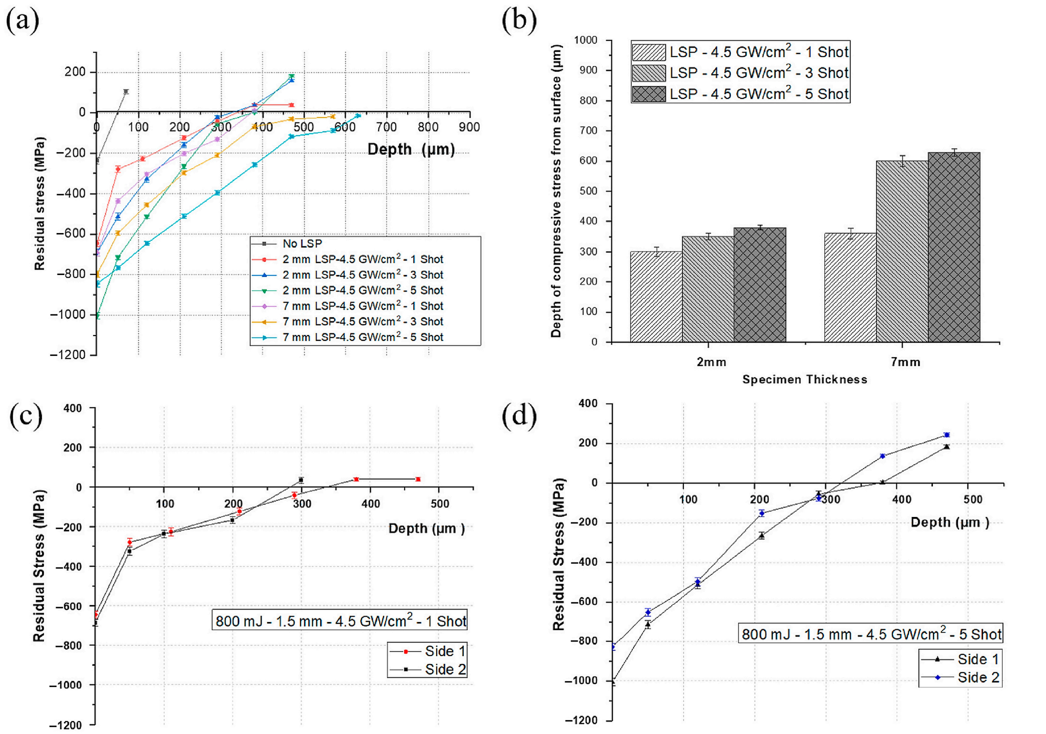

Figure 15. (**a**) Residual stress along the depth on specimens with different thicknesses subjected to LSP with varying laser shots; (**b**) depth of CRS in 2 mm and 7 mm specimens subjected to LSP on both sides with laser intensity 4.5 GW cm^{-2} (**c**) for one shot, and (**d**) five shot LSP [66].

Jinoop et al. [102] conducted a study on the LSP of Inconel 718 fabricated with additive laser manufacturing. One objective of the study was to determine the optimum laser power and number of shots for LSP. For this purpose, three different peak laser powers (140 mW, 170 mW, and 200 mW) and three shot numbers (3, 5, and 7) were considered and varied parametrically. The microhardness and depth profile values were determined based on the laser power and number of shot values. To determine the optimal parameters, a gray relational analysis was used with maximum hardness and minimum depth profile as the results. The determined laser power and number of shots are 170 mW and 7, respectively. This result means that moderate laser power and a higher number of shots are required to achieve both the lowest surface damage and the highest hardness value. With the optimal parameters, the tensile residual stress (197–227 MPa) of the sample in the raw state was completely converted to CRS (214.9–307.9 MPa) for the irradiated sample.

4. Performance Evaluation of LSP in PBF Materials

4.1. Hardness

Hardness is an important measure of the performance of materials. It is defined as a mechanical property that allows materials to resist plastic deformation. As explained in Section 2.1, the pressure of the shock wave in LSP treatment is on the order of GPa. This high pressure promotes plastic deformation, high dislocation density CRS, and grain refinement in the microstructure of the material. It is known from the dislocation strengthening theory that strain hardening can be produced by the generation and movement of dislocations [103] and from the Hall–Petch theory that there is a proportionality relationship between the microhardness value and the dislocation density [104].

The effectiveness of LSP in improving the hardness value of PBF materials has been studied by many researchers. For example, Hareharen et al. [92] studied the effects of LSP on the wear behavior, microstructure, residual stress distribution, and mechanical properties of 316 L stainless steel produced by SLM. As for microhardness, the measured hardness value for the initial sample is 226 $HV_{1.0}$, as shown in Figure 16. After LSP treatment, the hardness value increased to 276 $HV_{1.0}$ at the top surface.

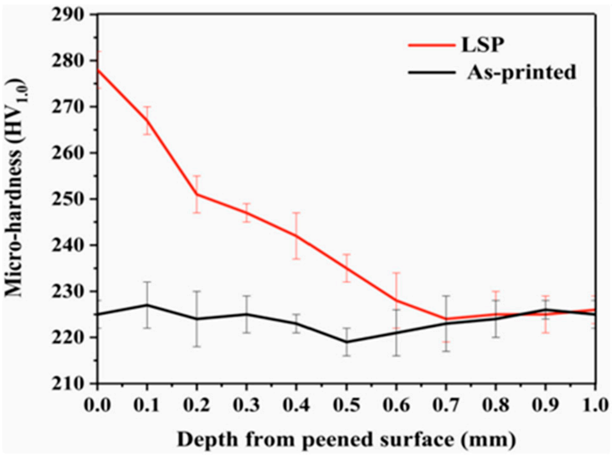

Figure 16. Microhardness results for as-built and LSP-treated samples [92].

Two studies were performed by Maleki et al. [76,86]. In the first study, a V-notched AlSi10Mg specimen built by LPBF were subjected to both T6 HT and LSP with two different laser beam energy (1.5 J and 4.5 J). From Figure 17a, it can be observed that the worst hardness value was measured on a heat-treated sample, which shows that T6 deteriorated the material hardening effect. The highest measured hardness value was 134 HV and it was obtained from the samples treated by LSP with 4.5 J. The LSP effect in this sample only disappeared up to a depth of 700 μm. This result means that a good microhardness value could be obtained without subjecting the additively manufactured samples to heat treatment prior to LSP. In the other investigation, the authors considered two different surface treatment methods, namely UNSM and LSP, which were applied to AlSi10Mg produced by

LPBF. To determine the posttreatment effect on AlSi10Mg mechanical properties, the same energy was used during the whole experiment. As shown in Figure 17b, the hardening effect from this study showed that for the as-built specimen, an average of 130 HV was obtained, which increased to 170 HV due to LSP application. This value further increased to over 200 HV when ultrasonic nanocrystalline surface modification (UNSM) treatment was applied individually and in conjunction with LSP treatment. Regarding the depth, the LSP effect could be observed to a depth up to 450 µm, whereas, for UNSM and LSP + UNSM, the effect of measured hardness value could be observed to a depth up to 850 µm and 200 µm. The effect of LSP on additively produced aluminum alloys was also investigated in another study, and a small increase in microhardness was found in the areas below the surface to a depth of about 300 µm [83].

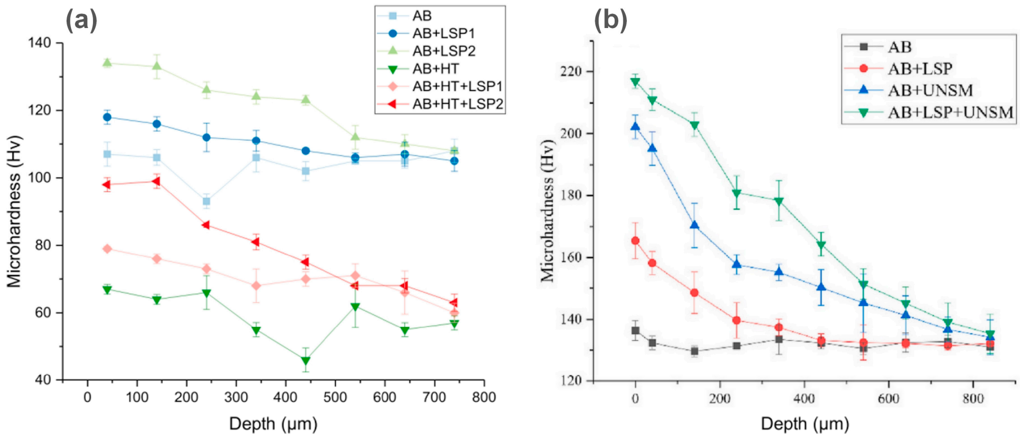

Figure 17. AlSi10Mg microhardness profiles along the depth (**a**) heat-treated sample (**b**) ultrasonic nanocrystalline surface treatment [76,86].

Another material commonly used in LSP studies is titanium alloy. For example, Inkyu Yeo et al. [81] performed LSP experiments on heat-treated Ti6A14V processed with LPBF to improve its surface properties. Three different laser energies were used to obtain the hardness: 1.9 GW, 5.7 GW, and 9.1 GW. The results of this study show that as the laser energy increases, the Vickers hardness value increases, with the highest recovery rate at 9.1 GW being 91.7%.

This study also found that HT lowers hardness. However, a different result was provided in a study by Chen et al. [91], which investigated the effects of HT and HT + LSP treatment on an Inconel 625 alloy produced by selective laser melting. The results showed that the value of microhardness increased by 19.5% after HT and by 32% after LSP compared to the unprinted sample. In addition, Ti6A14V fabricated by LPBF and subjected to massive LSP treatment was used to evaluate the effects of massive LSP treatment on the high-temperature oxidation resistance of the samples previously treated with AHT [58].

In this study, the LSP was applied to two different surfaces, one parallel to the substrate (0°) and one perpendicular to the substrate (90°). As can be seen from Figure 18a, the distribution of microhardness of all specimens shows that the improvement in microhardness by LSP is slightly higher at 0° than at 90°, whereas the measurements of microhardness along the depth direction show that the specimens subjected to hybrid treatment (AHT + MLSP) obtained better results both in terms of microhardness and depth, see Figure 18b.

Overall, a similar trend of microhardness reduction can be observed in both LPBF-MLSPTed and LPBF-AHT-MLSPTed. In all these studies, LSP treatment positively contributed to the improvement in the hardening properties of the additively manufactured materials, which was possible due to the grain refinement and CRS produced by LSP.

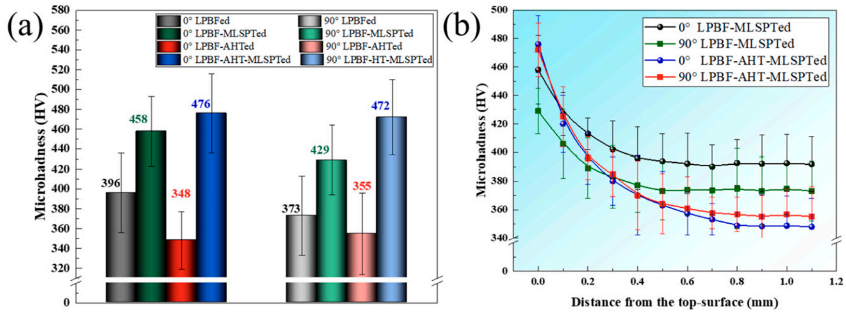

Figure 18. Microhardness results for all samples: (**a**) at the top surface and (**b**) along the depth direction [58].

4.2. Fatigue Life

In Section 2.1, it was mentioned that components fabricated with PBF have some defects that negatively affect fatigue strength. Although optimal parameters for PBF have been proposed, materials fabricated using traditional methods exhibit better fatigue strength than those fabricated using AM technology. For this reason, LSP is often used as a means to improve the fatigue strength of PBF materials. See Table 4 for a summary of results on fatigue strength improvement in PBF materials treated with LSP.

Soyama et al. [94] used several peening methods, namely submerged laser peening, which can also be termed laser cavitation peening, shot peening, and laser peening, to evaluate the fatigue improvement in Ti6Al4V titanium alloys fabricated using EBM. For this study, two cases were considered, with and without surface roughness, and the fatigue strength was determined using Little's method. In the analysis, a comparison was made between the untreated specimens and those treated with the peening methods. The results of the study showed that compared to the untreated specimens for the case without surface roughness, all peening treatments contributed to an increase in both fatigue life and strength, with the highest fatigue strength increase being shot peening with 98%, followed by laser peening with 87% and cavitation peening with 75%, as shown in Figure 19a. However, when the surface roughness is considered, better fatigue life is obtained from laser peening, followed by cavitation peening, and lastly shot peening, as illustrated in Figure 19b. In terms of fatigue strength improvement percentage between the untreated and the treated samples, an increase of 104% was obtained with laser peening, 84% for cavitation peening, and 68% with shot peening.

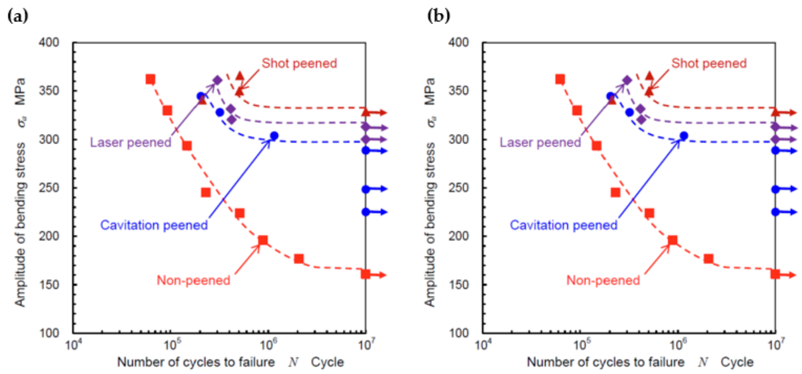

Figure 19. Fatigue strength improvement in Ti6Al4V fabricated by EBM by different peening techniques: (**a**) without surface roughness, (**b**) with surface roughness [94].

Table 4. Fatigue strength improvement in PBF materials treated with LSP.

Material	Laser Parameters	Fatigue Test	Load	Improvement Compared to AB Sample
316L SS [63]	10 ns, 3 mm (square spot), 4 J, 4.4 GW cm^{-2}	Four-point bending	350–500 MPa, $R = 1$	$4N_f$ (Vinyl tape as a confining layer) $1.9N_f$ (Al tape as a confining layer)
Ti-6A1-4V [94]	1064 nm, 10 Hz, 6 ns, 0.8 mm, 6 mm 0.35 J,	Bending	12 Hz, $R = -1$, ±15 Nm	87% (without surface roughness) 104% (with surface roughness)
AlSi7Mg [83]	1064 nm, 5 Hz, 6.3 ns, 50%, 1 mm, 1 J, 9 GW cm^{-2}	Three-point bending	200–300 MPa, 30 Hz, 4×10^4–5×10^6 cycles, $R = 0.1$	$50\%\sigma_f$
AlSi10Mg [76]	1064 nm, 10 Hz, 10 ns, 50%, 3 mm, 1.5 J and 4.5 J, 3 and 9 GW cm^{-2}	Rotating bending	110 MPa, 2550 rpm, 6×10^6 cycles, $R = -1$	$151N_f$ $199N_f$
AlSi10Mg [86]	1064 nm, 10 Hz, 10 ns, 50%, 3 mm, 4.5 J, 9 GW cm^{-2}	Rotating bending	110 MPa, 2550 rpm, 2×10^7 cycles, $R = -1$	$35N_f$
316L SS [105]	1064 nm, 5 Hz, 6.3 ns, 80%, 1 mm, 0.4 J, 8.1 GW cm^{-2}	Pure bending	120 Hz, $R = 0$	$14N_f$ (machined) $15N_f$ (non-machined)
316L SS [106]	18 ns, 3%, 4.7 mm (square spot), 4 GW cm^{-2}	Four-point bending	400–575 MPa, $R = 0.1$	60% (with notched) 80% (without notch)
Ti-6A1-4V [107]	1064 nm, 1 Hz, 12 ns, 25%, 11 GW cm^{-2}	Tension-tension	600–775 MPa, 15 Hz, 2×10^6 cycles, $R = 0.1$	$17\%\sigma_f$
TC17 [99]	1064 nm, 20 ns, 50%, 2.4 mm, 2.8 J	Tension-tension	15 Hz, $R = 0.1$	23.6%

In another study, Sohrabi et al. [87] performed a three-point bending fatigue investigation on LSP-treated Zr-based (AMZ4) bulk metal glass (BMG) fabricated using LPBF. Several conclusions were drawn from the results of this study: first, a lower fatigue limit was found for the as-received sample compared to reported values for Zr-based BMG. Second, no significant improvement in fatigue life was obtained for the LSP-treated specimens, but an increase in fatigue life by a factor of two was observed for loads greater than 250 MPa. Finally, it was also found that the fatigue behavior at lower loads was not affected by changing the build-up directions on the fabricated specimens, but resulted in a slight decrease in fatigue life for loads above 250 MPa.

All the fatigue results presented in Table 4 show that the application of the LSP treatment contributed to an increase in the lifetime of the PBF components. In all these cases, the main reason for the increase in fatigue life is the CRS generated by the LSP treatment. In a rotating fatigue test on AlSi10Mg performed using two different laser energies, it can be seen from Table 4 that a higher fatigue life was achieved with a higher laser energy (4.5 J).

4.3. Very High Cycle Fatigue

In practice, railroad wheels, for example, have been shown to fail at very high fatigue cycles (VHCF) [108] and components such as turbine blades experience 10^7 cycles due to their vibration loading during operation [109]. The development of ultrasonic testing systems capable of operating at frequencies of up to 30 KHz has increased the interest of researchers in testing materials with more than 10^7 cycles, the so-called "very high cycle fatigue regime". It is also of great interest to understand how LSP-treated materials behave under VHCF.

Qin et al. [110] investigated the effect of LSP on HCF and VHCF of 2024-T351 aluminum alloy. In this study, the specimens were treated with two different pulse energies of 10 J and 20 J, and an ultrasonic fatigue testing machine was used. As can be seen in Figure 20a, no fatigue limit was reached at 10^9 cycles for both the untreated and treated specimens. It can also be seen from the same graph that the fatigue life decreased after LSP treatment. Similar results were obtained in another study with the same LSP parameters, as shown in Figure 20b [111].

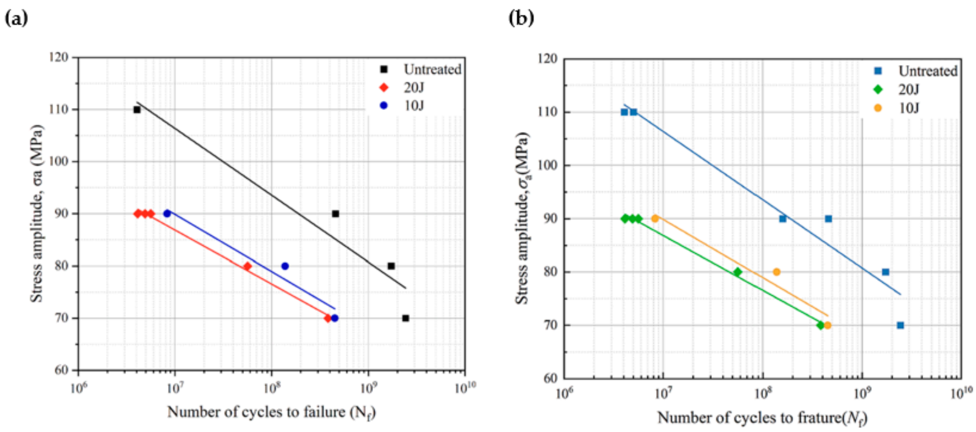

Figure 20. (**a**,**b**) Fatigue results of LSP treated and untreated samples [110,111].

These results are contrary to what one would expect from LSP treatment because it produces CRS, which counteracts the tensile residual stress that one would expect to extend the life of the treated materials. Another aspect of these two studies is that among the treated samples, the one with the lower pulse energy had a higher fatigue life. In another study, three different laser energies (2.6 J, 3.6 J, and 4.6 J) and two different exposure times (1 and 3) were applied to forged TC4 titanium [112]. The fatigue life from this study is shown in Figure 21. From the results, all treated specimens showed reasonable fatigue life in the range of HCF, with the best fatigue life obtained with 1-time impact, whereas after 10^7 cycles, the worst result was obtained with 4.6 J and 3-time impact.

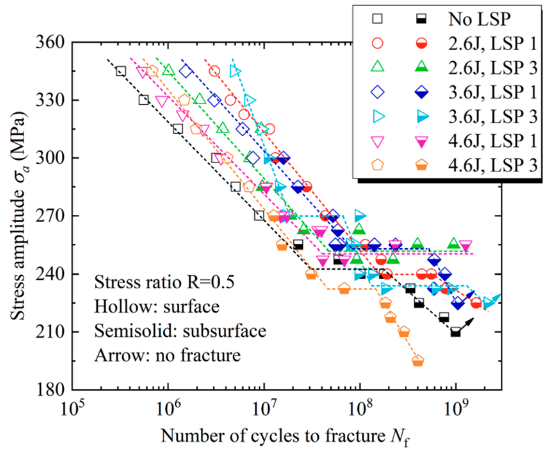

Figure 21. S-N curves of untreated and treated samples (different LSP treatments) [112].

Studies on the VHCF regime have also been performed on materials prepared with PBF [113–115]. However, the first study on LSP treatment of Ti6Al4V fabricated by SLM and subjected to the VHCF regime was performed by Jiang et al. [65]. In this study, the LSP treatment was applied to both sides of the samples and a laser energy of 7 J was considered. From the results, it was concluded that the LSP treatment was able to generate enough CRS to counteract the detrimental ones and cause grain refinement within the microstructure. Surprisingly, the untreated samples showed better fatigue results than the LSP-treated samples, as shown in Figure 22. The reasons for the lower S-N curve of the treated specimens were the inherent defects, increased surface roughness, and non-uniform residual stresses.

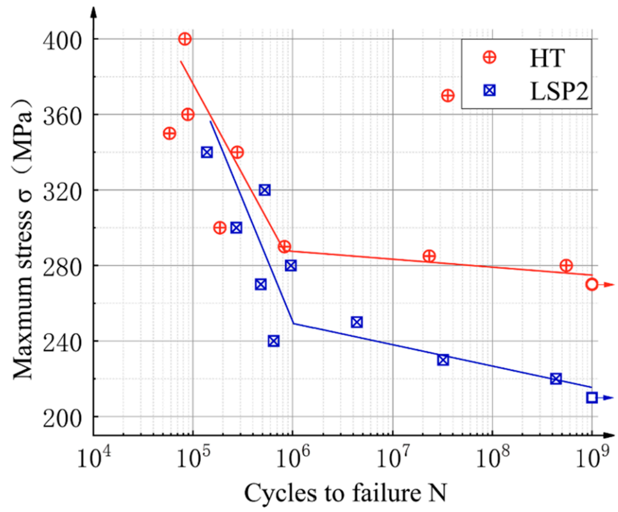

Figure 22. Fatigue life results before and after LSP [65].

5. Summary and Future Work Recommendation

The effectiveness of LSP has been proven for many materials manufactured by traditional methods such as machining, forming, casting, numerical computer control, etc. For additively manufactured materials, especially PBF materials, further experimental studies are needed to solidify the understanding of LSP. However, in this review, the latest results of LSP in PBF materials in terms of residual stress, hardness, fatigue life, and VHCF are presented and discussed.

From Table 2 a summary of LSP processing parameters applied on PBF materials is shown. Regarding the overlapping rate, in most studies, the value used ranges from 50% to 80%, which agrees well with the old literature that states that maximum efficiency is obtained when the overlapping range is between 50% and 70% [75]. From Table 2, it can also be concluded that for PBF materials, most LSP studies still include both constraint and sacrificial layers.

As for residual stress, most studies show that LSP treatment indeed promotes the formation of beneficial CRS, which contributes significantly to the improvement in the fatigue life of the components. As far as microhardness is concerned, all the studies consulted have shown a positive contribution to LSP.

In terms of fatigue life, the application of LSP to PBF materials resulted in an overall longer fatigue life of the treated material compared to the baseline condition, but most LSP studies on PBF materials do not include direct fatigue estimation and analysis. Some contradictory results have been observed on the tensile properties of PBF materials surface treated with LSP, which implies that more experiments should be conducted. As for VHCF, there are very few studies on the effects of LSP on fabricated PBF materials.

The performance of LSP surface treatment depends on the process parameters. Despite some studies on the optimization of process parameters, it is still a challenge to uniformly distribute CRS. In addition, there are very few studies on the optimization of LSP parameters of PBF materials. It is well known that components such as crankshafts, pressure vessels, turbines, and transmission systems are subjected to variable or random multiaxial loading conditions during operation. Therefore, it would also be interesting to test LSP-treated PBF material under multiaxial loading conditions. One way to consolidate the LSP method is to extend its application to more industrial components instead of focusing mainly on limited experiments.

Author Contributions: Conceptualization, F.B. and L.R.; methodology, F.B.; software, F.B.; validation, V.A., P.M. and R.B.; formal analysis, V.A.; investigation, F.B.; resources, L.R.; data curation, L.R.; writing—original draft preparation, F.B.; writing—review and editing, V.A.; visualization, F.B.; supervision, L.R. and V.A.; project administration, L.R. All authors have read and agreed to the published version of the manuscript.

Funding: This research received no external funding.

Acknowledgments: The authors gratefully acknowledge the support from FCT–Fundação para a Ciência e Tecnologia (Portuguese Foundation for Science and Technology), through IDMEC, under LAETA, project UIDB/50022/2020.

Conflicts of Interest: The authors declare no conflict of interest.

References

1. *ISO/ASTM 52900:2021*; Standard Terminology for Additive Manufacturing—General Principles—Terminology. ASTM International: West Conshohocken, PA, USA, 2021.
2. Blakey-Milner, B.; Gradl, P.; Snedden, G.; Brooks, M.; Pitot, J.; Lopez, E.; Leary, M.; Berto, F.; Du Plessis, A. Metal Additive Manufacturing in Aerospace: A Review. *Mater. Des.* **2021**, *209*, 110008. [CrossRef]
3. Pradeep, P.I.; Kumar, V.A.; Sriranganath, A.; Singh, S.K.; Sahu, A.; Kumar, T.S.; Narayanan, P.R.; Arumugam, M.; Mohan, M. Characterization and Qualification of LPBF Additively Manufactured AISI-316L Stainless Steel Brackets for Aerospace Application. *Trans. Indian Natl. Acad. Eng.* **2020**, *5*, 603–616. [CrossRef]
4. Vasco, J.C. Additive Manufacturing for the Automotive Industry. In *Additive Manufacturing*; Elsevier: Amsterdam, The Netherlands, 2021; pp. 505–530, ISBN 978-0-12-818411-0.
5. Chen, R.K.; Jin, Y.; Wensman, J.; Shih, A. Additive Manufacturing of Custom Orthoses and Prostheses—A Review. *Addit. Manuf.* **2016**, *12*, 77–89. [CrossRef]
6. Tilton, M.; Lewis, G.S.; Bok Wee, H.; Armstrong, A.; Hast, M.W.; Manogharan, G. Additive Manufacturing of Fracture Fixation Implants: Design, Material Characterization, Biomechanical Modeling and Experimentation. *Addit. Manuf.* **2020**, *33*, 101137. [CrossRef]
7. Vishnukumar, M.; Pramod, R.; Rajesh Kannan, A. Wire Arc Additive Manufacturing for Repairing Aluminium Structures in Marine Applications. *Mater. Lett.* **2021**, *299*, 130112. [CrossRef]

8. Global 3D Printing Metal Market Size & Trends Report 2030. Available online: https://www.grandviewresearch.com/industry-analysis/3d-metal-printing-market (accessed on 30 August 2023).
9. Additive Manufacturing Market Size Report 2030. Available online: https://www.grandviewresearch.com/industry-analysis/additive-manufacturing-market (accessed on 3 September 2023).
10. Niu, X.; Zhu, S.-P.; He, J.-C.; Liao, D.; Correia, J.A.F.O.; Berto, F.; Wang, Q. Defect Tolerant Fatigue Assessment of AM Materials: Size Effect and Probabilistic Prospects. *Int. J. Fatigue* **2022**, *160*, 106884. [CrossRef]
11. Liao, D.; Zhu, S.-P.; Keshtegar, B.; Qian, G.; Wang, Q. Probabilistic Framework for Fatigue Life Assessment of Notched Components under Size Effects. *Int. J. Mech. Sci.* **2020**, *181*, 105685. [CrossRef]
12. Gong, H.; Rafi, K.; Gu, H.; Starr, T.; Stucker, B. Analysis of Defect Generation in Ti–6Al–4V Parts Made Using Powder Bed Fusion Additive Manufacturing Processes. *Addit. Manuf.* **2014**, *1*, 87–98. [CrossRef]
13. Murr, L.E.; Quinones, S.A.; Gaytan, S.M.; Lopez, M.I.; Rodela, A.; Martinez, E.Y.; Hernandez, D.H.; Martinez, E.; Medina, F.; Wicker, R.B. Microstructure and Mechanical Behavior of Ti–6Al–4V Produced by Rapid-Layer Manufacturing, for Biomedical Applications. *J. Mech. Behav. Biomed. Mater.* **2009**, *2*, 20–32. [CrossRef]
14. Li, P.; Warner, D.H.; Fatemi, A.; Phan, N. Critical Assessment of the Fatigue Performance of Additively Manufactured Ti–6Al–4V and Perspective for Future Research. *Int. J. Fatigue* **2016**, *85*, 130–143. [CrossRef]
15. Moussaoui, K.; Rubio, W.; Mousseigne, M.; Sultan, T.; Rezai, F. Effects of Selective Laser Melting Additive Manufacturing Parameters of Inconel 718 on Porosity, Microstructure and Mechanical Properties. *Mater. Sci. Eng. A* **2018**, *735*, 182–190. [CrossRef]
16. Tillmann, W.; Schaak, C.; Nellesen, J.; Schaper, M.; Aydinöz, M.E.; Hoyer, K.-P. Hot Isostatic Pressing of IN718 Components Manufactured by Selective Laser Melting. *Addit. Manuf.* **2017**, *13*, 93–102. [CrossRef]
17. Hrabe, N.; Gnäupel-Herold, T.; Quinn, T. Fatigue Properties of a Titanium Alloy (Ti–6Al–4V) Fabricated via Electron Beam Melting (EBM): Effects of Internal Defects and Residual Stress. *Int. J. Fatigue* **2017**, *94*, 202–210. [CrossRef]
18. Uzan, N.E.; Shneck, R.; Yeheskel, O.; Frage, N. Fatigue of AlSi10Mg Specimens Fabricated by Additive Manufacturing Selective Laser Melting (AM-SLM). *Mater. Sci. Eng. A* **2017**, *704*, 229–237. [CrossRef]
19. Karimbaev, R.M.; Pyun, Y.-S.; Amanov, A. Fatigue Life Extension of Additively Manufactured Nickel-Base 718 Alloy by Nanostructured Surface. *Mater. Sci. Eng. A* **2022**, *831*, 142041. [CrossRef]
20. Maleki, E.; Bagherifard, S.; Bandini, M.; Guagliano, M. Surface Post-Treatments for Metal Additive Manufacturing: Progress, Challenges, and Opportunities. *Addit. Manuf.* **2021**, *37*, 101619. [CrossRef]
21. Lesyk, D.A.; Martinez, S.; Mordyuk, B.N.; Dzhemelinskyi, V.V.; Lamikiz, A.; Prokopenko, G.I. Post-Processing of the Inconel 718 Alloy Parts Fabricated by Selective Laser Melting: Effects of Mechanical Surface Treatments on Surface Topography, Porosity, Hardness and Residual Stress. *Surf. Coat. Technol.* **2020**, *381*, 125136. [CrossRef]
22. Chi, J.; Cai, Z.; Wan, Z.; Zhang, H.; Chen, Z.; Li, L.; Li, Y.; Peng, P.; Guo, W. Effects of Heat Treatment Combined with Laser Shock Peening on Wire and Arc Additive Manufactured Ti17 Titanium Alloy: Microstructures, Residual Stress and Mechanical Properties. *Surf. Coat. Technol.* **2020**, *396*, 125908. [CrossRef]
23. Du Plessis, A.; Glaser, D.; Moller, H.; Mathe, N.; Tshabalala, L.; Mfusi, B.; Mostert, R. Pore Closure Effect of Laser Shock Peening of Additively Manufactured AlSi10Mg. *3D Print. Addit. Manuf.* **2019**, *6*, 245–252. [CrossRef]
24. Ye, C.; Zhang, C.; Zhao, J.; Dong, Y. Effects of Post-Processing on the Surface Finish, Porosity, Residual Stresses, and Fatigue Performance of Additive Manufactured Metals: A Review. *J. Mater. Eng. Perform.* **2021**, *30*, 6407–6425. [CrossRef]
25. Kalainathan, S.; Prabhakaran, S. Recent Development and Future Perspectives of Low Energy Laser Shock Peening. *Opt. Laser Technol.* **2016**, *81*, 137–144. [CrossRef]
26. Zhang, X.; Ma, Y.; Yang, M.; Zhou, C.; Fu, N.; Huang, W.; Wang, Z. A Comprehensive Review of Fatigue Behavior of Laser Shock Peened Metallic Materials. *Theor. Appl. Fract. Mech.* **2022**, *122*, 103642. [CrossRef]
27. Qin, R.; Zhang, Z.; Hu, Z.; Du, Z.; Xiang, X.; Wen, G.; He, W. On-Line Evaluation and Monitoring Technology for Material Surface Integrity in Laser Shock Peening—A Review. *J. Mater. Process. Technol.* **2023**, *313*, 117851. [CrossRef]
28. Deng, W.; Wang, C.; Lu, H.; Meng, X.; Wang, Z.; Lv, J.; Luo, K.; Lu, J. Progressive Developments, Challenges and Future Trends in Laser Shock Peening of Metallic Materials and Alloys: A Comprehensive Review. *Int. J. Mach. Tools Manuf.* **2023**, *191*, 104061. [CrossRef]
29. Munther, M.; Martin, T.; Tajyar, A.; Hackel, L.; Beheshti, A.; Davami, K. Laser Shock Peening and Its Effects on Microstructure and Properties of Additively Manufactured Metal Alloys: A Review. *Eng. Res. Express* **2020**, *2*, 022001. [CrossRef]
30. Singh, S.N.; Deoghare, A.B. Laser Shock Peening of Laser Based Directed Energy Deposition and Powder Bed Fusion Additively Manufactured Parts: A Review. *Met. Mater. Int.* **2023**, *29*, 1563–1585. [CrossRef]
31. Mumtaz, K.; Hopkinson, N. Selective Laser Melting of Inconel 625 Using Pulse Shaping. *Rapid Prototyp. J.* **2010**, *16*, 248–257. [CrossRef]
32. Godec, D.; Gonzalez-Gutierrez, J.; Nordin, A.; Pei, E.; Ureña Alcázar, J. (Eds.) *A Guide to Additive Manufacturing*; Springer Tracts in Additive Manufacturing; Springer International Publishing: Cham, Switzerland, 2022; ISBN 978-3-031-05862-2.
33. Kruth, J.-P.; Deckers, J.; Yasa, E.; Wauthlé, R. Assessing and Comparing Influencing Factors of Residual Stresses in Selective Laser Melting Using a Novel Analysis Method. *Proc. Inst. Mech. Eng. Part B J. Eng. Manuf.* **2012**, *226*, 980–991. [CrossRef]

34. Carolo, L.C.B.; Cooper O., R. E. A Review on the Influence of Process Variables on the Surface Roughness of Ti-6Al-4V by Electron Beam Powder Bed Fusion. *Addit. Manuf.* **2022**, *59*, 103103. [CrossRef]
35. Herzog, D.; Seyda, V.; Wycisk, E.; Emmelmann, C. Additive Manufacturing of Metals. *Acta Mater.* **2016**, *117*, 371–392. [CrossRef]
36. Aboulkhair, N.T.; Everitt, N.M.; Ashcroft, I.; Tuck, C. Reducing Porosity in AlSi10Mg Parts Processed by Selective Laser Melting. *Addit. Manuf.* **2014**, *1*, 77–86. [CrossRef]
37. Dilip, J.J.S.; Zhang, S.; Teng, C.; Zeng, K.; Robinson, C.; Pal, D.; Stucker, B. Influence of Processing Parameters on the Evolution of Melt Pool, Porosity, and Microstructures in Ti-6Al-4V Alloy Parts Fabricated by Selective Laser Melting. *Prog. Addit. Manuf.* **2017**, *2*, 157–167. [CrossRef]
38. Jia, Q.; Gu, D. Selective Laser Melting Additive Manufacturing of Inconel 718 Superalloy Parts: Densification, Microstructure and Properties. *J. Alloys Compd.* **2014**, *585*, 713–721. [CrossRef]
39. Jia, Q.; Gu, D. Selective Laser Melting Additive Manufactured Inconel 718 Superalloy Parts: High-Temperature Oxidation Property and Its Mechanisms. *Opt. Laser Technol.* **2014**, *62*, 161–171. [CrossRef]
40. Sateesh, N.H.; Kumar, G.M.; Prasad, K.; Srinivasa, C.K.; Vinod, A.R. Microstructure and Mechanical Characterization of Laser Sintered Inconel-625 Superalloy. *Procedia Mater. Sci.* **2014**, *5*, 772–779. [CrossRef]
41. Buchbinder, D.; Schleifenbaum, H.; Heidrich, S.; Meiners, W.; Bültmann, J. High Power Selective Laser Melting (HP SLM) of Aluminum Parts. *Phys. Procedia* **2011**, *12*, 271–278. [CrossRef]
42. Olakanmi, E.O. Selective Laser Sintering/Melting (SLS/SLM) of Pure Al, Al–Mg, and Al–Si Powders: Effect of Processing Conditions and Powder Properties. *J. Mater. Process. Technol.* **2013**, *213*, 1387–1405. [CrossRef]
43. Sun, S.-H.; Koizumi, Y.; Saito, T.; Yamanaka, K.; Li, Y.-P.; Cui, Y.; Chiba, A. Electron Beam Additive Manufacturing of Inconel 718 Alloy Rods: Impact of Build Direction on Microstructure and High-Temperature Tensile Properties. *Addit. Manuf.* **2018**, *23*, 457–470. [CrossRef]
44. Podgornik, B.; Šinko, M.; Godec, M. Dependence of the Wear Resistance of Additive-Manufactured Maraging Steel on the Build Direction and Heat Treatment. *Addit. Manuf.* **2021**, *46*, 102123. [CrossRef]
45. Alsalla, H.H.; Smith, C.; Hao, L. Effect of Build Orientation on the Surface Quality, Microstructure and Mechanical Properties of Selective Laser Melting 316L Stainless Steel. *RPJ* **2018**, *24*, 9–17. [CrossRef]
46. Read, N.; Wang, W.; Essa, K.; Attallah, M.M. Selective Laser Melting of AlSi10Mg Alloy: Process Optimisation and Mechanical Properties Development. *Mater. Des.* **2015**, *65*, 417–424. [CrossRef]
47. Liang, X.; Hor, A.; Robert, C.; Lin, F.; Morel, F. Effects of Building Direction and Loading Mode on the High Cycle Fatigue Strength of the Laser Powder Bed Fusion 316L. *Int. J. Fatigue* **2023**, *170*, 107506. [CrossRef]
48. Edwards, P.; O'Conner, A.; Ramulu, M. Electron Beam Additive Manufacturing of Titanium Components: Properties and Performance. *J. Manuf. Sci. Eng.* **2013**, *135*, 061016. [CrossRef]
49. Takata, T.; Enoki, M.; Chivavibul, P.; Matsui, A.; Kobayashi, Y. Effect of Confinement Layer on Laser Ablation and Cavitation Bubble during Laser Shock Peening. *Mater. Trans.* **2016**, *57*, 1776–1783. [CrossRef]
50. Xiong, Q.; Shimada, T.; Kitamura, T.; Li, Z. Atomic Investigation of Effects of Coating and Confinement Layer on Laser Shock Peening. *Opt. Laser Technol.* **2020**, *131*, 106409. [CrossRef]
51. Ling, X.; Peng, W.; Ma, G. Influence of Laser Peening Parameters on Residual Stress Field of 304 Stainless Steel. *J. Press. Vessel Technol.* **2008**, *130*, 021201. [CrossRef]
52. Fabbro, R.; Fournier, J.; Ballard, P.; Devaux, D.; Virmont, J. Physical Study of Laser-Produced Plasma in Confined Geometry. *J. Appl. Phys.* **1990**, *68*, 775–784. [CrossRef]
53. Clauer, A.H.; Fairand, B.P.; Wilcox, B.A. Pulsed Laser Induced Deformation in an Fe-3 Wt Pct Si Alloy. *Met. Trans A* **1977**, *8*, 119–125. [CrossRef]
54. Thareja, R.K.; Shukla, S. Synthesis and Characterization of Zinc Oxide Nanoparticles by Laser Ablation of Zinc in Liquid. *Appl. Surf. Sci.* **2007**, *253*, 8889–8895. [CrossRef]
55. Guo, Y.B.; Caslaru, R. Fabrication and Characterization of Micro Dent Arrays Produced by Laser Shock Peening on Titanium Ti–6Al–4V Surfaces. *J. Mater. Process. Technol.* **2011**, *211*, 729–736. [CrossRef]
56. Leo, J.R.O.; Zabeen, S.; Fitzpatrick, M.E.; Zou, J.; Attallah, M.M. A Study on the Effects of Laser Shock Peening on the Microstructure and Substructure of Ti–6Al–4V Manufactured by Selective Laser Melting. *J. Mater. Process. Technol.* **2023**, *316*, 117959. [CrossRef]
57. Ruschau, J. Fatigue Crack Nucleation and Growth Rate Behavior of Laser Shock Peened Titanium. *Int. J. Fatigue* **1999**, *21*, 199–209. [CrossRef]
58. Wang, Z.; Huang, S.; Lu, H.; Liu, J.; Alexandrov, I.V.; Luo, K.; Lu, J. The Role of Annealing Heat Treatment in High-Temperature Oxidation Resistance of Laser Powder Bed Fused Ti6Al4V Alloy Subjected to Massive Laser Shock Peening Treatment. *Corros. Sci.* **2022**, *209*, 110732. [CrossRef]
59. Chen, L.; Sun, Y.; Li, L.; Ren, X. Microstructural Evolution and Mechanical Properties of Selective Laser Melted a Nickel-Based Superalloy after Post Treatment. *Mater. Sci. Eng. A* **2020**, *792*, 139649. [CrossRef]
60. Cheng, G.J.; Shehadeh, M.A. Dislocation Behavior in Silicon Crystal Induced by Laser Shock Peening: A Multiscale Simulation Approach. *Scr. Mater.* **2005**, *53*, 1013–1018. [CrossRef]
61. Montross, C.S.; Florea, V.; Swain, M.V. The Influence of Coatings on Subsurface Mechanical Properties of Laser Peened 2011-T3 Aluminum. *J. Mater. Sci.* **2001**, *36*, 1801–1807. [CrossRef]

62. Zhou, Z.; Bhamare, S.; Ramakrishnan, G.; Mannava, S.R.; Langer, K.; Wen, Y.; Qian, D.; Vasudevan, V.K. Thermal Relaxation of Residual Stress in Laser Shock Peened Ti–6Al–4V Alloy. *Surf. Coat. Technol.* **2012**, *206*, 4619–4627. [CrossRef]
63. Zulić, S.; Rostohar, D.; Kaufman, J.; Pathak, S.; Kopeček, J.; Böhm, M.; Brajer, J.; Mocek, T. Fatigue Life Enhancement of Additive Manufactured 316l Stainless Steel by LSP Using a DPSS Laser System. *Surf. Eng.* **2022**, *38*, 183–190. [CrossRef]
64. Pathak, S.; Zulić, S.; Kaufman, J.; Kopeček, J.; Stránský, O.; Böhm, M.; Brajer, J.; Beránek, L.; Shukla, A.; Ackermann, M.; et al. Post-Processing of Selective Laser Melting Manufactured SS-304L by Laser Shock Peening. *J. Mater. Res. Technol.* **2022**, *19*, 4787–4792. [CrossRef]
65. Jiang, Q.; Li, S.; Zhou, C.; Zhang, B.; Zhang, Y. Effects of Laser Shock Peening on the Ultra-High Cycle Fatigue Performance of Additively Manufactured Ti6Al4V Alloy. *Opt. Laser Technol.* **2021**, *144*, 107391. [CrossRef]
66. Ramadas, H.; Sarkar, S.; Ganesh, P.; Kaul, R.; Majumdar, J.D.; Nath, A.K. Enhancing the Static and Dynamic Mechanical Properties of Laser Powder Bed Fusion Process Built 15–5 Precipitation Hardening Stainless Steel Specimens by Laser Shock Peening. *Mater. Sci. Eng. A* **2023**, *866*, 144657. [CrossRef]
67. Sathyajith, S.; Kalainathan, S. Effect of Laser Shot Peening on Precipitation Hardened Aluminum Alloy 6061-T6 Using Low Energy Laser. *Opt. Lasers Eng.* **2012**, *50*, 345–348. [CrossRef]
68. Cao, Y.; Shin, Y.C.; Wu, B. A Parametric Study on Overlapping Laser Shock Peening of 4140 Steel via Modeling and Experiments. In Proceedings of the ASME 2008 International Manufacturing Science and Engineering Conference, Evanston, IL, USA, 7–10 October 2008; ASMEDC: Evanston, IL, USA, 2008; Volume 1, pp. 245–254.
69. Hong, X.; Wang, S.; Guo, D.; Wu, H.; Wang, J.; Dai, Y.; Xia, X.; Xie, Y. Confining Medium and Absorptive Overlay. *Opt. Lasers Eng.* **1998**, *29*, 447–455. [CrossRef]
70. Mannava, S.; McDaniel, A.; Cowie, W.; Halila, H.; Rhoda, J.; Gutknecht, J. Laser Shock Peening Gas Turbine Fan Blade Edges. US Patent US5591009A, 7 January 1997.
71. Yoda, M.; Newton, B. Underwater Laser Peening. In Proceedings of the Welding and Repair Technology for Power Plants Eighth International EPRI Conference, Fort Myers, FL, USA, 18–20 June 2008.
72. Withers, P.J.; Bhadeshia, H.K.D.H. Residual Stress. Part 1—Measurement Techniques. *Mater. Sci. Technol.* **2001**, *17*, 355–365. [CrossRef]
73. Guo, J.; Fu, H.; Pan, B.; Kang, R. Recent Progress of Residual Stress Measurement Methods: A Review. *Chin. J. Aeronaut.* **2021**, *34*, 54–78. [CrossRef]
74. Bastola, N.; Jahan, M.P.; Rangasamy, N.; Rakurty, C.S. A Review of the Residual Stress Generation in Metal Additive Manufacturing: Analysis of Cause, Measurement, Effects, and Prevention. *Micromachines* **2023**, *14*, 1480. [CrossRef] [PubMed]
75. Praveenkumar, K.; Sudhagara Rajan, S.; Swaroop, S.; Manivasagam, G. Laser Shock Peening: A Promising Tool for Enhancing the Aeroengine Materials' Surface Properties. *Surf. Eng.* **2023**, *39*, 245–274. [CrossRef]
76. Maleki, E.; Bagherifard, S.; Unal, O.; Bandini, M.; Guagliano, M. On the Effects of Laser Shock Peening on Fatigue Behavior of V-Notched AlSi10Mg Manufactured by Laser Powder Bed Fusion. *Int. J. Fatigue* **2022**, *163*, 107035. [CrossRef]
77. Montross, C. Laser Shock Processing and Its Effects on Microstructure and Properties of Metal Alloys: A Review. *Int. J. Fatigue* **2002**, *24*, 1021–1036. [CrossRef]
78. Kalentics, N.; Boillat, E.; Peyre, P.; Ćirić-Kostić, S.; Bogojević, N.; Logé, R.E. Tailoring Residual Stress Profile of Selective Laser Melted Parts by Laser Shock Peening. *Addit. Manuf.* **2017**, *16*, 90–97. [CrossRef]
79. Karbalaian, H.R.; Yousefi-Koma, A.; Karimpour, M.; Mohtasebi, S.S. Investigation on the Effect of Overlapping Laser Pulses in Laser Shock Peening with Finite Element Method. *Procedia Mater. Sci.* **2015**, *11*, 454–458. [CrossRef]
80. Luo, K.Y.; Lin, T.; Dai, F.Z.; Luo, X.M.; Lu, J.Z. Effects of Overlapping Rate on the Uniformities of Surface Profile of LY2 Al Alloy during Massive Laser Shock Peening Impacts. *Surf. Coat. Technol.* **2015**, *266*, 49–56. [CrossRef]
81. Yeo, I.; Bae, S.; Amanov, A.; Jeong, S. Effect of Laser Shock Peening on Properties of Heat-Treated Ti–6Al–4V Manufactured by Laser Powder Bed Fusion. *Int. J. Precis. Eng. Manuf. Green Technol.* **2021**, *8*, 1137–1150. [CrossRef]
82. Sohrabi, N.; Ran, R.; Duro, P.A.; Cayron, C.; Jhabvala, J.; Pejchal, V.; Sereda, O.; Logé, R.E. Laser Powder-Bed Fusion of a High Entropy Alloy with Outstanding Intrinsic Mechanical Properties. *J. Alloys Compd.* **2023**, *945*, 169209. [CrossRef]
83. Hamidi-Nasab, M.; Vedani, M.; Logé, R.; Sohrabi, N.; Jamili, A.M.; Du Plessis, A.; Beretta, S. An Investigation on the Fatigue Behavior of Additively Manufactured Laser Shock Peened Alsi7mg Alloy Surfaces. *SSRN J.* **2022**, *200*, 112907. [CrossRef]
84. Sandmann, P.; Keller, S.; Kashaev, N.; Ghouse, S.; Hooper, P.A.; Klusemann, B.; Davies, C.M. Influence of Laser Shock Peening on the Residual Stresses in Additively Manufactured 316L by Laser Powder Bed Fusion: A Combined Experimental–Numerical Study. *Addit. Manuf.* **2022**, *60*, 103204. [CrossRef]
85. Morgano, M.; Kalentics, N.; Carminati, C.; Capek, J.; Makowska, M.; Woracek, R.; Maimaitiyili, T.; Shinohara, T.; Loge, R.; Strobl, M. Investigation of the Effect of Laser Shock Peening in Additively Manufactured Samples through Bragg Edge Neutron Imaging. *Addit. Manuf.* **2020**, *34*, 101201. [CrossRef]
86. Maleki, E.; Bagherifard, S.; Unal, O.; Jam, A.; Shao, S.; Guagliano, M.; Shamsaei, N. Superior Effects of Hybrid Laser Shock Peening and Ultrasonic Nanocrystalline Surface Modification on Fatigue Behavior of Additive Manufactured AlSi10Mg. *Surf. Coat. Technol.* **2023**, *463*, 129512. [CrossRef]

87. Sohrabi, N.; Hamidi-Nasab, M.; Rouxel, B.; Jhabvala, J.; Parrilli, A.; Vedani, M.; Logé, R.E. Fatigue Performance of an Additively Manufactured Zr-Based Bulk Metallic Glass and the Effect of Post-Processing. *Metals* **2021**, *11*, 1064. [CrossRef]
88. Bian, H.; Wang, Z.; Liu, J.; Lu, H.; Luo, K.; Lu, J. Laser Shock Wave-Induced Enhanced Thermal Corrosion Resistance of Ti6Al4V Alloy Fabricated by Laser Powder Bed Fusion. *Surf. Coat. Technol.* **2023**, *452*, 129096. [CrossRef]
89. Lv, J.; Luo, K.; Lu, H.; Wang, Z.; Liu, J.; Lu, J. Achieving High Strength and Ductility in Selective Laser Melting Ti-6Al-4V Alloy by Laser Shock Peening. *J. Alloys Compd.* **2022**, *899*, 163335. [CrossRef]
90. Deng, W.W.; Lu, H.F.; Xing, Y.H.; Luo, K.Y.; Lu, J.Z. Effect of Laser Shock Peening on Tensile Properties and Microstructure of Selective Laser Melted 316L Stainless Steel with Different Build Directions. *Mater. Sci. Eng. A* **2022**, *850*, 143567. [CrossRef]
91. Chen, L.; Gu, P.; Ge, T.; Sun, Y.; Li, L.; Ren, X. Effect of Laser Shock Peening on Microstructure and Mechanical Properties of TiC Strengthened Inconel 625 Alloy Processed by Selective Laser Melting. *Mater. Sci. Eng. A* **2022**, *835*, 142610. [CrossRef]
92. Hareharen, K.; Kumar, P.; Panneerselvam, T.; Babu, D.; Sriraman, N. Investigating the Effect of Laser Shock Peening on the Wear Behaviour of Selective Laser Melted 316L Stainless Steel. *Opt. Laser Technol.* **2023**, *162*, 109317. [CrossRef]
93. Kalentics, N.; Sohrabi, N.; Tabasi, H.G.; Griffiths, S.; Jhabvala, J.; Leinenbach, C.; Burn, A.; Logé, R.E. Healing Cracks in Selective Laser Melting by 3D Laser Shock Peening. *Addit. Manuf.* **2019**, *30*, 100881. [CrossRef]
94. Soyama, H.; Okura, Y. The Use of Various Peening Methods to Improve the Fatigue Strength of Titanium Alloy Ti6Al4V Manufactured by Electron Beam Melting. *AIMS Mater. Sci.* **2018**, *5*, 1000–1015. [CrossRef]
95. Lan, L.; Xin, R.; Jin, X.; Gao, S.; He, B.; Rong, Y.; Min, N. Effects of Laser Shock Peening on Microstructure and Properties of Ti–6Al–4V Titanium Alloy Fabricated via Selective Laser Melting. *Materials* **2020**, *13*, 3261. [CrossRef]
96. Guo, W.; Sun, R.; Song, B.; Zhu, Y.; Li, F.; Che, Z.; Li, B.; Guo, C.; Liu, L.; Peng, P. Laser Shock Peening of Laser Additive Manufactured Ti6Al4V Titanium Alloy. *Surf. Coat. Technol.* **2018**, *349*, 503–510. [CrossRef]
97. Lu, J.Z.; Luo, K.Y.; Zhang, Y.K.; Cui, C.Y.; Sun, G.F.; Zhou, J.Z.; Zhang, L.; You, J.; Chen, K.M.; Zhong, J.W. Grain Refinement of LY2 Aluminum Alloy Induced by Ultra-High Plastic Strain during Multiple Laser Shock Processing Impacts. *Acta Mater.* **2010**, *58*, 3984–3994. [CrossRef]
98. Lu, J.Z.; Luo, K.Y.; Zhang, Y.K.; Sun, G.F.; Gu, Y.Y.; Zhou, J.Z.; Ren, X.D.; Zhang, X.C.; Zhang, L.F.; Chen, K.M.; et al. Grain Refinement Mechanism of Multiple Laser Shock Processing Impacts on ANSI 304 Stainless Steel. *Acta Mater.* **2010**, *58*, 5354–5362. [CrossRef]
99. Luo, S.; He, W.; Chen, K.; Nie, X.; Zhou, L.; Li, Y. Regain the Fatigue Strength of Laser Additive Manufactured Ti Alloy via Laser Shock Peening. *J. Alloys Compd.* **2018**, *750*, 626–635. [CrossRef]
100. Sun, J.; Li, J.; Chen, X.; Xu, Z.; Lin, Y.; Jiang, Q.; Chen, J.; Li, Y. Optimizing Parameters with FEM Model for 20CrMnTi Laser Shocking. *Materials* **2022**, *16*, 328. [CrossRef]
101. Wu, J.; Li, Y.; Qiao, H.; Yang, Y.; Zhao, J.; Huang, Z. Prediction of Mechanical Properties and Surface Roughness of FGH4095 Superalloy Treated by Laser Shock Peening Based on XGBoost. *J. Alloys Metall. Syst.* **2023**, *1*, 100001. [CrossRef]
102. Jinoop, A.N.; Subbu, S.K.; Paul, C.P.; Palani, I.A. Post-Processing of Laser Additive Manufactured Inconel 718 Using Laser Shock Peening. *Int. J. Precis. Eng. Manuf.* **2019**, *20*, 1621–1628. [CrossRef]
103. Qiao, H.; Zhao, J.; Gao, Y. Experimental Investigation of Laser Peening on TiAl Alloy Microstructure and Properties. *Chin. J. Aeronaut.* **2015**, *28*, 609–616. [CrossRef]
104. Chu, J.P.; Rigsbee, J.M.; Banaś, G.; Elsayed-Ali, H.E. Laser-Shock Processing Effects on Surface Microstructure and Mechanical Properties of Low Carbon Steel. *Mater. Sci. Eng. A* **1999**, *260*, 260–268. [CrossRef]
105. Kalentics, N.; Boillat, E.; Peyre, P.; Gorny, C.; Kenel, C.; Leinenbach, C.; Jhabvala, J.; Logé, R.E. 3D Laser Shock Peening—A New Method for the 3D Control of Residual Stresses in Selective Laser Melting. *Mater. Des.* **2017**, *130*, 350–356. [CrossRef]
106. Hackel, L.; Rankin, J.R.; Rubenchik, A.; King, W.E.; Matthews, M. Laser Peening: A Tool for Additive Manufacturing Post-Processing. *Addit. Manuf.* **2018**, *24*, 67–75. [CrossRef]
107. Jin, X.; Lan, L.; Gao, S.; He, B.; Rong, Y. Effects of Laser Shock Peening on Microstructure and Fatigue Behavior of Ti–6Al–4V Alloy Fabricated via Electron Beam Melting. *Mater. Sci. Eng. A* **2020**, *780*, 139199. [CrossRef]
108. Nanninga, N.E. Fatigue Crack Initiation and Fatigue Life of Metals Exposed to Hydrogen. In *Gaseous Hydrogen Embrittlement of Materials in Energy Technologies*; Elsevier: Amsterdam, The Netherlands, 2012; pp. 347–378. ISBN 978-1-84569-677-1.
109. Murakami, Y.; Nomoto, T.; Ueda, T.; Murakami, Y. On the Mechanism of Fatigue Failure in the Superlong Life Regime (N > 107 Cycles). Part 1: Influence of Hydrogen Trapped by Inclusions. *Fatigue Fract. Eng. Mater. Struct.* **2000**, *23*, 893–902. [CrossRef]
110. Qin, Z.; Li, B.; Huang, X.; Zhang, H.; Chen, R.; Adeel, M.; Xue, H. The Effect of Laser Shock Peening on Surface Integrity and High and Very High Cycle Fatigue Properties of 2024-T351 Aluminum Alloy. *Opt. Laser Technol.* **2022**, *149*, 107897. [CrossRef]
111. Li, B.; Qin, Z.; Zhang, H.; Xue, H. The Effects of Laser Peening Treatment on the Very High Cycle Fatigue Properties for AA2024-T351 Alloy Using a Crystal Plasticity Framework. *Eng. Fract. Mech.* **2022**, *275*, 108840. [CrossRef]
112. Wang, B.; Cheng, L.; Li, D. Study on Very High Cycle Fatigue Properties of Forged TC4 Titanium Alloy Treated by Laser Shock Peening under Three-Point Bending. *Int. J. Fatigue* **2022**, *156*, 106668. [CrossRef]
113. Voloskov, B.; Evlashin, S.; Dagesyan, S.; Abaimov, S.; Akhatov, I.; Sergeichev, I. Very High Cycle Fatigue Behavior of Additively Manufactured 316L Stainless Steel. *Materials* **2020**, *13*, 3293. [CrossRef] [PubMed]

114. Wycisk, E.; Siddique, S.; Herzog, D.; Walther, F.; Emmelmann, C. Fatigue Performance of Laser Additive Manufactured Ti–6Al–4V in Very High Cycle Fatigue Regime up to 109 Cycles. *Front. Mater.* **2015**, *2*, 72. [CrossRef]
115. Qian, G.; Li, Y.; Paolino, D.S.; Tridello, A.; Berto, F.; Hong, Y. Very-High-Cycle Fatigue Behavior of Ti-6Al-4V Manufactured by Selective Laser Melting: Effect of Build Orientation. *Int. J. Fatigue* **2020**, *136*, 105628. [CrossRef]